

Article

# On the Conceptual Design of Novel Supercritical CO<sub>2</sub> Power Cycles for Waste Heat Recovery

Giovanni Manente <sup>1,\*</sup>  and Mário Costa <sup>2</sup> <sup>1</sup> Department of Industrial Engineering, University of Padova, via Venezia 1, 35131 Padova, Italy<sup>2</sup> IDMEC, Mechanical Engineering Department, Instituto Superior Técnico, Universidade de Lisboa, Av. Rovisco Pais 1, 1049-001 Lisboa, Portugal; mcosta@tecnico.ulisboa.pt

\* Correspondence: G.Manente@bham.ac.uk; Tel.: +44-789-531-5084

Received: 24 November 2019; Accepted: 9 January 2020; Published: 12 January 2020



**Abstract:** The supercritical CO<sub>2</sub> power cycle (s-CO<sub>2</sub>) is receiving much interest in the utilization of waste heat sources in the medium-to-high temperature range. The low compression work and highly regenerative layout result in high thermal efficiencies, even at moderate turbine inlet temperatures. The capability of heat extraction from the waste heat source is, however, limited because the heat input takes place over a limited temperature range close to the maximum cycle temperature. Accordingly, novel s-CO<sub>2</sub> layouts have been recently proposed, aimed at increasing the heat extraction from the heat source while preserving as much as possible the inherently high thermal efficiency. Among these, the most promising ones feature dual expansion, dual recuperation, and partial heating. This work concentrates on the conceptual design of these novel s-CO<sub>2</sub> layouts using a systematic approach based on the superimposition of elementary thermodynamic cycles. The overall structure of the single flow split with dual expansion (also called cascade), partial heating, and dual recuperated cycles is decomposed into elementary Brayton cycles to identify the building blocks for the achievement of a high performance in the utilization of waste heat sources. A thermodynamic optimization is set up to compare the performance of the three novel layouts for utilization of high temperature waste heat at 600 °C. The results show that the single flow split with a dual expansion cycle provides 3% and 15% more power compared to the partial heating and dual recuperated cycles, respectively, and 40% more power compared to the traditional single recuperated cycle used as the baseline. The separate evaluation of thermal efficiency and heat recovery effectiveness shows the main reasons behind the achievement of the highest performance, which are peculiar to each novel layout.

**Keywords:** supercritical CO<sub>2</sub> power cycles; waste heat recovery; partial heating; dual recuperated; dual expansion; cascade

## 1. Introduction

### 1.1. The s-CO<sub>2</sub> Power Cycle for Recovery of High Temperature Waste Heat

The recovery of waste heat for mechanical and electrical power generation is among the key strategies to reduce the consumption of fossil fuels and limit CO<sub>2</sub> emissions. The Paris Agreement on climate change and the Special Report on global warming of 1.5 °C published in October 2018 by the Intergovernmental Panel on Climate Change (IPCC) demonstrate the worldwide commitment to control global warming. In this context, the EU recently revised upwards (from 27% to 32.5%) the target for 2030 about the improvement in energy efficiency. Several recent studies assessed the amount and quality of waste heat potential in several sectors and countries. Forman et al. [1] assessed the waste heat potential in the electricity generation sector and in the most common sectors of end use. The authors showed that, globally, 38% of the waste heat in the industrial sector, 36% in the commercial sector,

and 54% in the transportation sector are available at temperatures higher than 300 °C. Focusing on the industrial waste heat in the EU, Papapetrou et al. [2] found that the waste heat potential at temperatures higher than 500 °C amounts to 124 TWh/year, which represents 41% of the total. Vance et al. [3] estimated the potential and barriers for waste heat recovery (WHR) at temperatures higher than 650 °C in five industries (steel, aluminum, glass, cement, and lime). The authors pointed out that reactive constituents, often present in the waste gases from these industries, may complicate the heat recovery process and require new technologies. They estimated a potential for WHR from these high temperature streams in the U.S. equal to 113.6 TWh/year. Firth et al. [4] forecasted the global waste heat emissions in 2030 from the power generation, industry, transport, and building sectors. Their analysis suggested an important need for effective medium and high temperature WHR technologies.

All these studies point to a huge amount of wasted heat at high temperatures that could be conveniently converted into electricity with high thermal efficiencies. However, there appears to be a lack of consensus about the best technology to accomplish this goal. The supercritical CO<sub>2</sub> (s-CO<sub>2</sub>) power cycle represents a promising option due to the high thermal efficiency, scalability to low power ranges (hundreds of kW), small footprint, and favorable economics. The s-CO<sub>2</sub> cycle was originally proposed by Feher [5] and Angelino [6] to overcome the thermodynamic and technological limitations of the Rankine and Brayton cycles. Both authors suggested nuclear power as the foremost application, as also considered by Dostal [7] in his popular doctoral thesis, which still represents one of the most comprehensive studies on “traditional” s-CO<sub>2</sub> power cycle layouts. In the meantime, the renewed interest in concentrating solar power and, in particular, on the central receiver layout suggested the s-CO<sub>2</sub> power cycle as a suitable power block substitute for the Rankine cycle due to its higher thermal efficiency and compactness. Since the beginning of this last decade, many efforts have been devoted to extending its range of application to other fields, especially in the recovery of waste heat, where the maximization of net power output rather than of thermal efficiency is to be pursued. In this field, three main approaches are considered. The first one simply takes the traditional s-CO<sub>2</sub> layouts and optimizes their cycle parameters for maximum power. The second one considers a sequence of two traditional s-CO<sub>2</sub> layouts in a cascade utilization of the waste heat. The third one suggests novel layouts specifically developed to overcome the limitations of the traditional layouts in heat extraction from the waste heat source. In the following, the main findings and results obtained from the applications of these approaches in the literature are summarized, to ultimately focus on the third approach.

### 1.2. Traditional s-CO<sub>2</sub> Power Cycles for WHR

The traditional s-CO<sub>2</sub> layouts generally considered in the literature for WHR applications are the single recuperated, recompression, and pre-compression layouts, and the objective function is the net power output or, in relative terms, the ratio between the net power output and overall heat available from the heat source from the inlet temperature to the ambient temperature, called the “total heat recovery efficiency”. One of the most enlightening studies was performed by Mohagheghi and Kapat [8], who optimized the net power output of the single recuperated and recompression s-CO<sub>2</sub> power cycles for WHR in a wide temperature range between 230 and 830 °C. The authors showed that the optimum recompression cycle reduces to the single recuperated layout for waste gas temperatures lower than 450 °C, whereas it only marginally improves the power output at higher temperatures. The authors highlighted the high gap between the waste gas inlet temperature and optimum turbine inlet temperature (TIT), and the high outlet temperature of the waste heat source (stack temperature). These drawbacks were found to be more pronounced at high waste gas temperatures and for the recompression layout. A different finding was obtained by Khadse et al. [9] for a waste gas at 630 °C. The authors showed that the recompression cycle improves by 22.9% the power output of the single recuperated cycle. This result is probably ascribable to the different assumptions compared to the previous study, in particular the higher maximum pressure (33 MPa). Moroz et al. [10] extended the performance comparison to the pre-compression cycle and a wide set of gas turbines having exhaust temperatures in the range 450–650 °C. For a gas temperature of 550 °C, the maximum total heat

recovery efficiency of 21.3% reached by the single recuperated cycle exceeds by 2% that achieved by the recompression and pre-compression layouts. The authors claimed that the lower CO<sub>2</sub> temperatures at the inlet of the Heater of the single recuperated cycle imply, on the one hand, a lower thermal efficiency but, on the other hand, a more effective heat extraction from the waste gas. Martinez et al. [11] evaluated the same three traditional cycles for WHR from a gas turbine having an exhaust temperature of 600 °C. They found that the single recuperated cycle improves by a few percentage points the power output of the recompression cycle and by several percentage points that of the pre-compression cycle. This is the outcome of the higher heat recovery effectiveness (called the WHR efficiency), which prevails over the lower cycle thermal efficiency.

The majority of these studies share the main result that the single recuperated cycle is the best choice among the traditional layouts for WHR applications. Contextually, they point out that the application of traditional layouts for WHR generates a mismatch between the heat source and power cycle at the higher temperature level, and the inability to acquire heat at the lower temperature level, which results in significant exergy destruction and exergy losses, respectively.

### 1.3. Cascade of Two Traditional s-CO<sub>2</sub> Power Cycles for WHR

The combination of two traditional cycles in a cascaded system is considered by many authors as the best solution to solve the two aforementioned main limitations of the single cycle. In the cascaded system, the higher temperature waste heat usually feeds the recompression cycle, whereas the residual waste heat is used to generate additional power in a single recuperated cycle, as also proposed by one of the authors [12] for the recovery of flue gas from biomass combustion. Hou et al. [13] evaluated the performance of a combined s-CO<sub>2</sub> system composed of the sequence of a recompression cycle and a single recuperated cycle that share the same compressor for WHR from a marine gas turbine having an exhaust temperature of 534 °C. The optimum solution obtained from a multi-objective optimization showed that the cascaded system enables a contextually high maximum temperature of the recompression cycle and a quite low gas outlet temperature to be reached, which ultimately results in a significant increment of power output (approximately 30%) compared to a single cycle. Zhang et al. [14] optimized the performance of a similar cascaded system for WHR from the exhaust gases at 490 °C of an offshore gas turbine, which basically differs from the previous one by allowing two different maximum cycle pressures. The solution obtained from a multi-objective optimization using the net power output and levelized energy cost as objective functions showed that the optimum cycle pressures reach the upper bounds (15 and 20 MPa). Moroz et al. [15] used the single recuperated, recompression, and basic non-recuperated cycles as building blocks to propose new configurations of cascaded s-CO<sub>2</sub> power cycles. In the “composite” schemes devised by the authors, the different cycles share some equipment (e.g., compressor, cooler, recuperator) to reduce the number of plant components. The authors show that the composite cycles improve by 24.7% to 31.7% the power output of the single recuperated cycle in the WHR of exhaust gases at 471 °C. This is due to the better capability of heat extraction from the exhaust gases, as demonstrated by the much lower stack temperature (90–130 °C in the novel schemes versus 210 °C of the single recuperated cycle). Different combinations were also explored in the literature, where the organic Rankine cycle (ORC) substitutes for the second s-CO<sub>2</sub> cycle in the cascaded system. For instance, Hou et al. [16] proposed a novel system composed of the sequence of a single recuperated s-CO<sub>2</sub> cycle and an ORC using zeotropic mixtures of cyclopentane (cC5) and refrigerant R365mfc for WHR from a regenerative gas turbine. The authors carried out multi-objective optimization using the exergy efficiency and cost of electricity of the entire system as objective functions. They showed that the replacement of the single recuperated cycle with a recompression or a basic non-recuperated s-CO<sub>2</sub> cycle would worsen both the thermodynamic and economic performance. Cao et al. [17] proposed a combined system composed of the sequence of a basic non-recuperated s-CO<sub>2</sub> cycle and a transcritical CO<sub>2</sub> cycle for WHR from a gas turbine. The transcritical cycle receives heat from the exhaust of the s-CO<sub>2</sub> cycle and from the residual heat of the flue gases and uses the liquefied natural gas as a heat sink. The results of the thermodynamic

optimization obtained for a small gas turbine having an exhaust temperature of 510 °C showed that the basic s-CO<sub>2</sub> cycle already enables an effective cooling of the flue gases, hence the main function of the transcritical CO<sub>2</sub> cycle is the recovery of the heat available at the discharge of the s-CO<sub>2</sub> cycle.

These studies clearly show the thermodynamic advantage of a cascaded system composed of traditional cycles, which can improve by up to 30% the net power output of a single s-CO<sub>2</sub> cycle in WHR applications. On the other hand, they also highlight their major criticality, namely the high number of required components, in spite of the very recent efforts to address this point, as shown by the cascaded layouts with shared equipment.

#### 1.4. Novel s-CO<sub>2</sub> Power Cycles for WHR

The novel s-CO<sub>2</sub> power cycle layouts devised in the last decade for WHR applications provide a high performance with a comparatively lower number of components compared to the cascaded systems described in the previous section. The most relevant ones are here referred to as the “single flow split with dual expansion”, “dual flow split with dual expansion”, and “dual recuperated” s-CO<sub>2</sub> power cycles. They apparently resemble a traditional s-CO<sub>2</sub> cycle but differ from the latter by including two turbines. Among the s-CO<sub>2</sub> layouts specifically developed for WHR applications, it is the “partial heating cycle” that can still provide a high performance using a single turbine.

One of the first studies published about novel s-CO<sub>2</sub> power cycles for WHR was an EPRI (Electric Power Research Institute) report by Kimzey [18], who presented and optimized the performance of three novel s-CO<sub>2</sub> power cycles for WHR from gas turbines, selected out of nearly 30 configurations initially conceived. The first one is the single flow split with dual expansion (called baseline Cascade Cycle 1), which was first presented during a conference by a cutting-edge company [19]. The other two cycles were proposed by the author as an advancement on the baseline cycle and include the more complex layout with dual flow split and dual expansion. Focusing on the first novel cycle, the author showed that it can provide a 1.5% to 3% gain in power output compared to a two-pressure level steam bottoming cycle, whereas it is outperformed by the triple pressure with reheat steam cycle commonly used for larger heavy duty gas turbines. The authors showed that its main drawback is the poor thermal profile match in the low temperature recuperator, which implies an incomplete recovery of the heat at the exhaust of the CO<sub>2</sub> turbines. Another early study on advanced s-CO<sub>2</sub> layouts was that by Walnum et al. [20], who, referring to a patent by Held et al. [21], compared the performance of the novel dual recuperated (called “dual stage”) s-CO<sub>2</sub> power cycle against that of a single recuperated cycle for WHR from a 32 MW gas turbine installed in an offshore platform. At the design point, the authors found that the dual recuperated cycle improves the power output of the single recuperated cycle by 10.1%. This is mainly a result of the enhanced heat extraction from the heat source, as demonstrated by the lower flue gas outlet temperature (125 versus 170 °C), and the higher cycle maximum temperature (426 versus 365 °C) attained by the dual recuperated cycle. In the latter, approximately 40% of the total CO<sub>2</sub> mass flow rate is heated by the exhaust of the high temperature turbine (HTT) in a high temperature recuperator (HTR), and directly expanded in the low temperature turbine (LTT). The partial heating (often called “preheating”) cycle completes the picture of the most relevant novel layouts and was selected by Wright et al. [22] as one of the most promising s-CO<sub>2</sub> power cycles for WHR applications. The authors maximized the net annual revenue by searching for the optimum cycle parameters, in particular the turbine inlet temperature and split flow fraction, and the optimum heat exchanger approach temperatures. For each cycle, they evaluated the separate contributions of the cycle thermal efficiency and heat recovery effectiveness at the optimum point. They found that the 17.1% to 22.6% gain in the net power output of the novel cycles over the single recuperated cycle is accompanied by a 10.1% to 17.6% increment in the specific investment cost. Among the novel cycles, the highest rate of return (15.6%) was achieved by the dual recuperated cycle.

These first promising results paved the way for further studies aimed at comparing the performance of the novel s-CO<sub>2</sub> power cycles against that attainable by single or cascaded layouts of traditional s-CO<sub>2</sub> cycles or multi-pressure steam cycles. In this context, one of the earliest and most comprehensive

study is by Cho et al. [23], who compared the performance of the novel s-CO<sub>2</sub> power cycles proposed by Kimzey [18] against that attainable by cascaded systems composed of the sequence of recompression or pre-compression and partial heating cycles. In the WHR from a gas turbine having an exhaust temperature of 580 °C, the authors found that the dual flow split with a dual expansion cycle improves by 6.6% to 8.5% the power generated by the cascaded s-CO<sub>2</sub> systems, and even improves by 3.6% the power output of a triple pressure with a reheat steam cycle. Even though the single flow split with dual expansion provided only 85% of the power output of the dual flow split cycle, it was considered a promising option due to the lower number of heat exchangers and turbomachinery. Also based on these findings, Huck et al. [24] exclusively focused on the dual flow split with a dual expansion layout and compared its performance against that achievable by state-of-the-art steam bottoming cycles for heavy-duty and aeroderivative gas turbines. The author found that this advanced s-CO<sub>2</sub> power cycle can perform even better than a three-pressure reheat steam cycle provided that maximum CO<sub>2</sub> pressures exceeding 30 MPa are allowed, and considering very high efficiencies (95%) for CO<sub>2</sub> turbomachinery. Instead, a 0.5% gain in the combined cycle efficiency is attainable when this s-CO<sub>2</sub> layout replaces the dual pressure non-reheat steam cycle also using the more accessible assumptions of a near-term design. Kim M.S. et al. [25] extended the comparison to a wider set of s-CO<sub>2</sub> power cycle layouts for WHR from a 5.0 MW gas turbine. Besides the traditional layouts (single recuperated, recompression, and pre-compression), they considered the partial heating cycle, three novel layouts with dual expansion proposed by Kimzey [18], and three original concepts. They found that the partial heating cycle improves by 23.3% to 26.2% the power output generated by the traditional layouts and even marginally improves by 2.6% the power generated by the single flow split with a dual expansion cycle. The power output of the latter was found to be equal to 83% to 86% of that achievable by the dual flow split with a dual expansion cycle, which is consistent with Cho et al. [23]. On the other hand, the new concepts devised by the authors could not exceed the power output achieved by the partial heating cycle, which was finally considered the most promising option for a megawatt scale due to the simpler layout, smaller number of components, and simpler operational scheme. A more focused study on this layout was carried out by Kim Y.M. et al. [26], who compared the performance of the partial heating cycle (called “split flow”) against that of the single recuperated cycle for WHR from a 25 MW gas turbine. The authors evaluated the separate contributions of the cycle thermal efficiency and heat recovery effectiveness in the calculation of the total heat recovery efficiency (called the “system thermal efficiency”). They showed that the maximum total heat recovery efficiency reaches 26.0% for the partial heating cycle, which is 6% higher than the maximum attained by the single recuperated cycle. This is mainly the result of the higher heat recovery effectiveness (89.6% versus 69.2%), with the cycle thermal efficiency remaining almost unaltered. The authors showed that in both cycles, the optimum TIT (in the range 390–400 °C) is much lower than the exhaust gas temperature (538 °C), which implies high exergy losses in the heater. The performance of the partial heating cycle was found to be even better than that of a cascaded system composed of the sequence of two single recuperated cycles, in spite of the lower number of components. Marchionni et al. [27] carried out a techno-economic comparison between four traditional s-CO<sub>2</sub> power cycle layouts against four layouts specifically developed for WHR applications. The latter included the partial heating s-CO<sub>2</sub> cycle (called preheating) and one novel layout proposed by the authors, which differs from the partial heating cycle by including a pre-compressor. In the utilization of flue gas at 650 °C, the authors found that the novel layouts outperform the traditional ones. Even though the comparison between novel layouts may be partially biased by the assumption a fixed flue gas outlet temperature (150 °C), the maximum power output was achieved by the partial heating cycle with or without the pre-compressor plant modification.

In summary, these studies agree about the unrivalled performance of the dual flow split with a dual expansion cycle but, virtually, suggest the partial heating cycle and the single flow split with a dual expansion cycle as the most promising layouts due to their relevant performance and simpler layouts.

With the only exception of Wright et al. [22], the performance assessment of the dual recuperated layout is limited to a comparison against traditional s-CO<sub>2</sub> cycles. One of the most relevant studies

on this novel layout is by Wu et al. [28], who optimized the performance of dual recuperated cycles (called “dual stage”) for WHR from exhaust gases with inlet temperatures in the range 250–500 °C. For the highest exhaust temperature of 500 °C, the dual recuperated cycle was found to improve by 4.5% the total heat recovery efficiency of the single recuperated cycle (i.e., 23.22% versus 18.77%). Furthermore, the highest performance was obtained at maximum pressures that were a few MPa lower than the corresponding ones for the single recuperated cycle. The authors showed that the performance of the dual recuperated cycle could be only marginally improved (less than 0.5%) by the addition of a third turbine and third recuperator. The performance comparison was extended to economic aspects in the recent study by Wang et al. [29], who carried out a thermodynamic and exergoeconomic optimization of a dual recuperated s-CO<sub>2</sub> power cycle for WHR from a 2.9 MW internal combustion engine. The significant improvement in the net power output (22.2%) and the almost negligible increase in the cost compared to the single recuperated cycle obtained after the multi-objective optimization made the dual recuperated cycle the recommended choice. Instead, the addition of a third turbine and recuperator stage was found to be detrimental from both aspects. Astolfi et al. [30] recently evaluated the performance of the dual recuperated cycle (called “cascade recuperative”) for WHR in a wide temperature range between 200 and 600 °C. The authors showed that this layout always provides a higher power output than the single recuperated and recompression cycles for the utilization of waste heat sources having a high cooling grade. In particular, in the absence of any constraint on the minimum heat source outlet temperature, the total heat recovery efficiency was found to reach approximately 25% for a waste heat source at 550 °C.

Thus, it clearly appears from these studies that the dual recuperated cycle has a high potential to improve the performance of traditional s-CO<sub>2</sub> layouts in WHR applications. The claimed 22% to 24% gain in power compared to the single recuperated cycle closely matches that attainable by the single flow split with dual expansion and partial heating layouts having a similar complexity. So, an important need stands out for a systematic comparison between these three novel layouts based on a common basis to extend the study by Wright et al. [22]. A prerequisite to that is a deeper understanding of the topology of each power system, i.e., the way in which constituent parts (equipment) are interrelated or arranged.

### *1.5. Decomposition of Complex Plants into Elementary Thermodynamic Cycles*

Advanced layouts of power cycles are not easily comprehensible. The rationale behind the sequence of basic plant components and the design of heat transfer network within the system is not within everyone’s reach. The inventors of novel plant layouts often conceal the basic idea leading to a new plant proposal. To make the comprehension of advanced layouts easier, a method was conceived within the research group of the present first author, which traces the origin of the new layouts to the well-known Rankine and Brayton cycles. At the beginning, the method was merely applied to understand the genesis of advanced layouts based on the gas turbine. More recently, it has been codified in an algorithm to automatically generate new layouts of power cycles. The main development stages are briefly summarized in the following. In the proposal and application of the Heatsep method, Lazzaretto and Toffolo [31] showed that the synthesis of energy system configurations can be considered as an operation in which one or more thermodynamic cycles are composed into a single system. These cycles may be open or closed and the working fluids may be different. The different cycles may be separated, as in a combined gas/steam combined cycle, or partially superimposed, as in a steam gas injected gas turbine (STIG) or humid air turbine cycle (HAT). They share common transformations after their working fluids are merged (e.g., using mixers) and their common paths end when the streams are separated in other components (e.g., in splitters or condensers). In a further study, Lazzaretto and Manente [32] showed that the advanced oxy-combustion cycles, like the S-Graz or the H<sub>2</sub>/O<sub>2</sub> power cycles, can be thought of as the superimposition of Brayton cycles operated by steam and/or CO<sub>2</sub> and steam Rankine cycles with high temperature reheat and three expansion stages. Even though the analysis remained at a descriptive level, the authors could identify a clear evolution of the layouts of

the elementary thermodynamic cycles, which goes in the direction of improving the thermal efficiency of both the Brayton and Rankine cycles composing the overall system. However, the improvement of the thermal efficiency does not suffice, and should be accompanied by the enhanced capability of heat recovery from the hot streams available within the system. This point was addressed by Morandin et al. [33], who analyzed the steam injected gas turbine (STIG) cycle as the combination of two partially superimposed cycles, namely an air Brayton cycle and a steam Rankine cycle. The authors first calculated the thermal efficiency of each elementary cycle disregarding any thermal interaction between them, as if the heat input to the elementary steam cycle was entirely provided by a fictitious external heat source. In this way, they could introduce the “baseline” thermal efficiency concept, as the mass flow rate weighted average of the thermal efficiencies of the two elementary cycles. The real thermal efficiency of the STIG cycle was then calculated as the sum of the baseline thermal efficiency and an efficiency gain (mainly) related to the internal heat recovery. The authors showed that the main effect in the evolution towards more advanced STIG plant configurations featuring high and low pressure steam turbines is the increase of the baseline thermal efficiency. More recently Lazzaretto et al. [34] developed an automatic procedure for the synthesis of energy system configurations (called “Synthsep”), which consists in two steps. In the first step, all meaningful system configurations are generated by combining two or more elementary Rankine cycles by sharing (partially or totally) one or more of their thermodynamic processes using a comprehensive and rigorous set of rules. In the second step, a two-level optimization is performed to select the system configuration and the associated design parameters leading to the highest value of the objective function. The authors applied this method for the synthesis/design optimization of a dual pressure ORC system using iC4 and R245fa. They found that the optimum system layout is obtained when the two elementary Rankine cycles have shared expansion and cooling processes. While the algorithm has been developed so far by Toffolo [35] for Rankine cycle-based energy systems only, yet this general approach could be extended to Brayton cycle-based energy systems as well.

These studies show that the decomposition of advanced power cycles in elementary thermodynamic cycles could be a useful tool not only to identify the building blocks of the system but also for its preliminary assessment. Indeed, the calculation of the thermal efficiency of each elementary cycle could provide a first indication about the overall performance of the system, though the latter is highly affected by the thermal interactions between elementary cycles.

### *1.6. Aim and Main Novelty of This Work*

This work deals with a systematic analysis and thermodynamic optimization of three novel s-CO<sub>2</sub> power cycles for waste heat recovery, which are selected as the most promising due to their high performance and low number of components. They are referred to in this work as single flow split with dual expansion, partial heating, and dual recuperated cycles, even though they might be known to the reader under different names (cascade, preheating, and dual stage or split cycles, respectively). The thermodynamic performance of the power cycles is optimized using the power output as the objective function and a coherent set of assumptions to allow for a fair comparison. The heat source is assumed available at an inlet temperature of 600 °C, which is considered as a benchmark temperature for recovery of high temperature waste heat in the industrial sector (steel industry, etc.) as well as in the electricity sector (gas turbines, fuel cells, etc.). Each advanced layout is decomposed into two elementary thermodynamic cycles, which are partially superimposed. The two cycles join after the mixer, follow a common path, and separate after the splitter. To the authors' knowledge, such a decomposition of advanced s-CO<sub>2</sub> power cycle layouts into elementary Brayton cycles has never been explored in the literature. An attempt is made to identify in them the features of a topping cycle, which receives heat from the waste heat source, and a bottoming cycle, fed by the exhaust of the topping cycle. The thermal efficiency of each elementary cycle is calculated to quantify the separate contribution of each elementary cycle composing the system to the output power in the cascade utilization of the waste heat.

With the only exception of the work by Wright et al. [22], these three layouts have never been compared to each other in a single study, and this is done for the first time on the basis of a pure thermodynamic objective. Moreover, unlike [22] and almost all studies in the literature, which focus on the optimum point, this work shows a wider spectrum of design options that include the optimum one as a particular solution. The overall performance is explained based on two metrics, namely the “cycle thermal efficiency” and the “heat recovery effectiveness”, following the approach recently used by one of the current authors in the comparison of traditional s-CO<sub>2</sub> layouts and two novel s-CO<sub>2</sub> layouts with dual expansion [36]. The former represents the capability of the novel power cycles in heat to power conversion, and the latter quantifies their ability in extracting heat from the waste heat source. This decomposition of the overall performance into two metrics highlights the strengths and weaknesses of each layout and helps understand the trend of the variation of the power output with the decision variables, which is peculiar to each layout.

## 2. Materials and Methods

The methodology used in this work consists of the following four steps: (1) Selection of the most suitable s-CO<sub>2</sub> power cycles for the WHR application; (2) analysis of their layouts to understand their genesis and building blocks; (3) setting of a common and sound basis for thermodynamic optimization and comparison; and (4) breakdown of the overall performance into meaningful elementary sub-metrics. The final goal was to gain a deeper insight into the underlying reasons leading to high performance and provide new directions of development for advanced s-CO<sub>2</sub> power cycles for WHR.

### 2.1. Selection and Analysis of s-CO<sub>2</sub> Power Cycles for WHR: Layouts and Decomposition into Elementary Thermodynamic Cycles

Following a thorough literature survey on s-CO<sub>2</sub> power cycles for WHR briefly outlined in the introduction, three layouts were selected, which combine a high potential with a relatively simple configuration and low number of components. The single flow split with dual expansion cycle was already selected by one of the present authors in [36], whereas the partial heating and dual recuperated cycles were first selected by the authors in this study. For each layout, an effort was made to disaggregate the overall structure into elementary thermodynamic cycles, which helps to understand the genesis of these advanced systems.

#### 2.1.1. Single Flow Split with Dual Expansion s-CO<sub>2</sub> Power Cycle

Figure 1 shows the layout of the single flow split with dual expansion s-CO<sub>2</sub> cycle [36]. The total CO<sub>2</sub> flow at the outlet of the compressor (state 2) is split into two streams. The first stream ( $m_1$ ) is heated to the maximum cycle temperature (state 3) in the heater and expanded in the high temperature turbine, HTT (3–4). The second stream ( $m_2$ ) is heated to the inlet temperature of the low temperature turbine, LTT (state 7), in two recuperators (LTR and HTR) in sequence. The CO<sub>2</sub> flow leaving the HTT is cooled in the HTR (4–5) and mixed with the exhaust from LTT. The total CO<sub>2</sub> flow is cooled in the LTR (9–10) and cooler (10–1) down to the desired compressor inlet state.

This highly integrated system can be thought of as being composed of two partially superimposed elementary Brayton cycles: A topping non-recuperated cycle (Figure 2a) and a bottoming recuperated cycle (Figure 2b). The two elementary thermodynamic cycles share the cooler and the compressor and interact through the HTR and LTR. In the topping cycle, CO<sub>2</sub> is heated from the compressor outlet to the inlet of the HTT by the external heat source. In the bottoming cycle, CO<sub>2</sub> is heated from the compressor outlet to the inlet of the LTT primarily by recovering the exhaust heat from the HTT (in HTR and LTR) and, partially, by recovering the exhaust heat from the LTT (in LTR). Thus, the LTR has a double function: Not only does it recover the low temperature exhaust heat from the topping cycle but it also recovers internally the exhaust heat within the bottoming cycle.

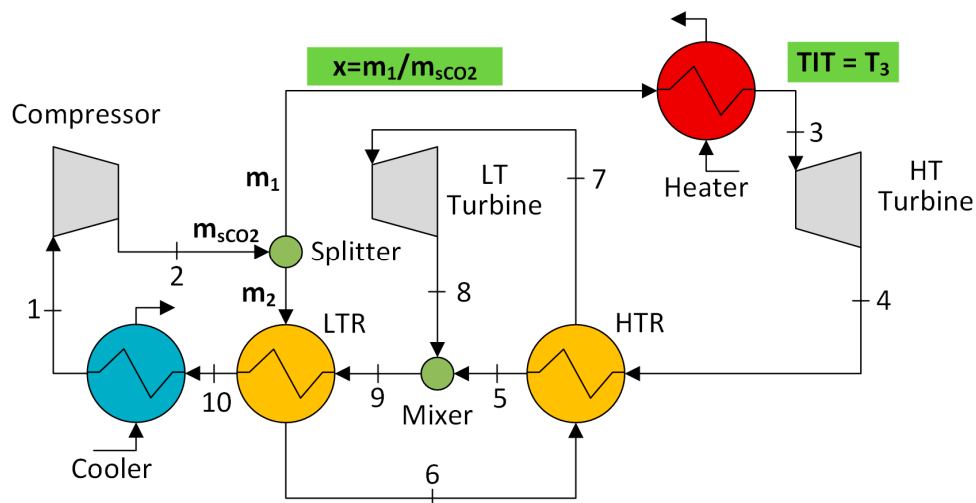


Figure 1. Single flow split with dual expansion s-CO<sub>2</sub> cycle [36].

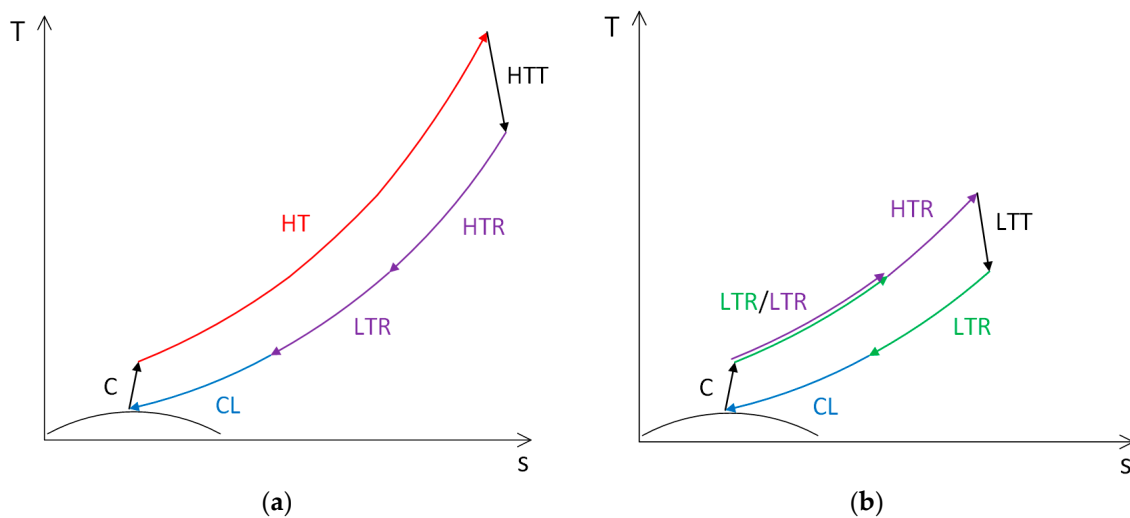


Figure 2. Decomposition of the single flow split with a dual expansion s-CO<sub>2</sub> cycle into two elementary thermodynamic cycles: (a) First elementary cycle (topping); (b) Second elementary cycle (bottoming).

In the schematic representation of the elementary cycles in Figure 2, the thermodynamic processes are drawn using different colors. The red color refers to the heat input from the external heat source, the blue to the heat rejection to the environment, the green to the regenerative heat transfer within each elementary thermodynamic cycle, and the violet to the heat transfer from the topping to the bottoming elementary cycle.

### 2.1.2. Partial Heating s-CO<sub>2</sub> Power Cycle

Figure 3 shows the layout of the partial heating s-CO<sub>2</sub> cycle. The total CO<sub>2</sub> flow at the outlet of the compressor is split into two streams that are heated in parallel to an intermediate temperature. The first stream ( $m_1$ ) is heated to state 3 by the external heat source in heater 1, whereas the second stream ( $m_2$ ) is heated to state 4 in the recuperator by recovering internally the heat at the turbine exhaust. After mixing (state 5), the total CO<sub>2</sub> flow is heated by the external heat source in the heater 2 (5–6) up to the turbine inlet temperature. The turbine exhaust is cooled in the recuperator (7–8) and in the cooler (8–1) in sequence down to the desired compressor inlet state.

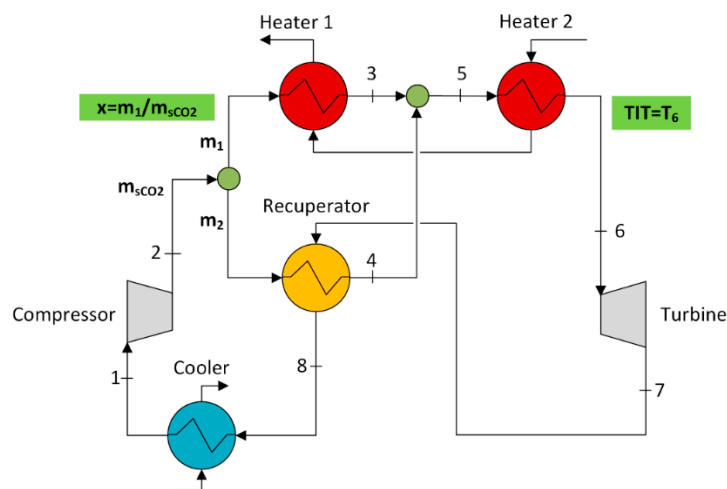


Figure 3. Partial heating s-CO<sub>2</sub> cycle.

The partial heating cycle can still be thought of as being composed of two elementary Brayton cycles, both operating between the minimum and maximum cycle temperature and sharing most of the equipment. The first elementary thermodynamic cycle (Figure 4a) is a non-recuperated cycle and fully acts as a topping cycle because it receives heat from the external heat source in heater 1 and heater 2 and makes the heat at the turbine exhaust available for recovery. The second elementary cycle (Figure 4b) is a recuperated cycle (see the green processes) that only partially acts as a bottoming cycle. Indeed, besides recovering heat from the topping cycle in the recuperator (at the lower temperature level, violet process), it also receives heat directly from the external heat source in the heater 2 (at the higher temperature level, red process).

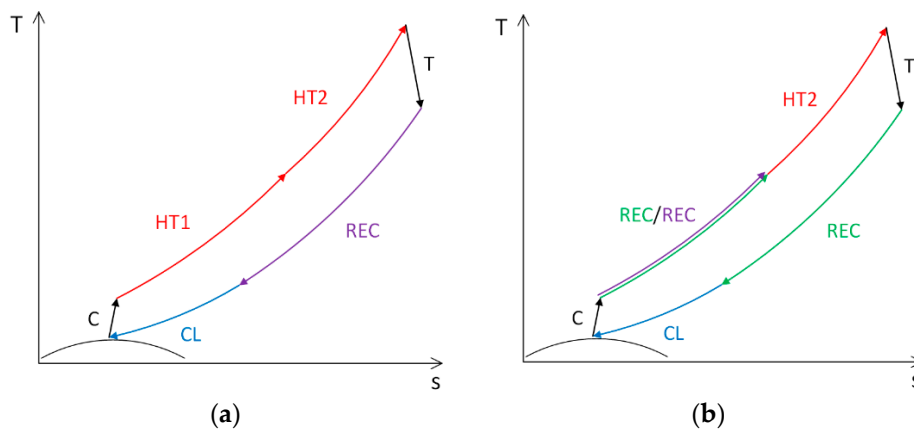


Figure 4. Decomposition of the partial heating s-CO<sub>2</sub> cycle into two elementary thermodynamic cycles: (a) First elementary cycle (topping); (b) Second elementary cycle.

### 2.1.3. Dual Recuperated s-CO<sub>2</sub> Power Cycle

Figure 5 shows the layout of the dual recuperated s-CO<sub>2</sub> cycle. The CO<sub>2</sub> flow at the outlet of the compressor is split into two streams that are sent to two recuperators in parallel (LTR and HTR). The first stream ( $m_1$ ) is heated in the LTR by the exhaust of the LTT and, subsequently, in the heater by the external heat source before expansion in the HTT. The second stream ( $m_2$ ) is heated in the HTR by the exhaust of the HTT before expansion in the LTT. After heat recovery in the HTR (5–6) and in the LTR (8–9), the two heat depleted exhaust streams are mixed, and the residual heat is rejected to the environment in the cooler (10–1) down to the desired compressor inlet state.

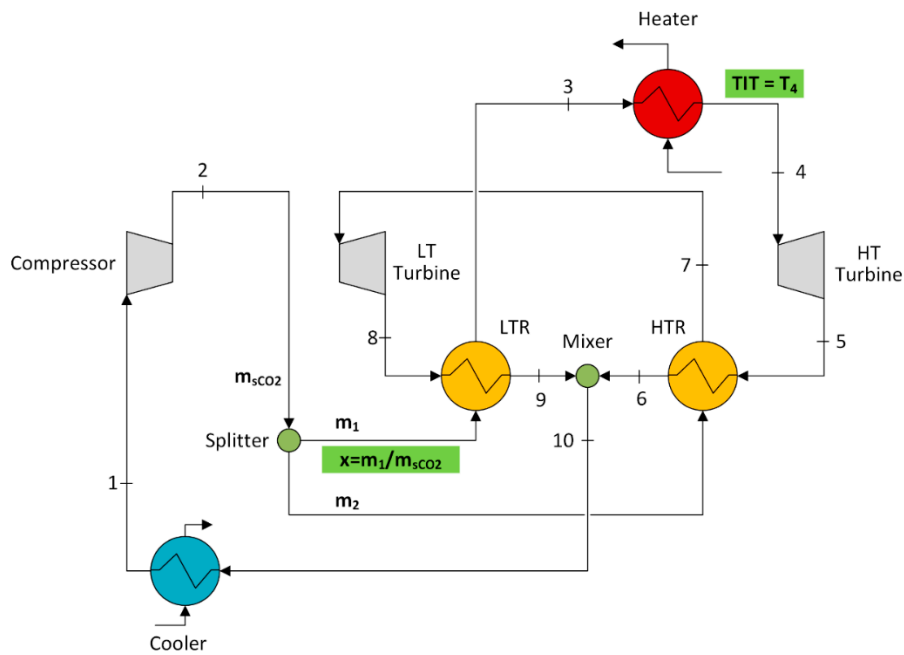


Figure 5. Dual recuperated s-CO<sub>2</sub> cycle.

Even though the distinct features of a topping and bottoming cycle cannot be strictly identified, the dual recuperated s-CO<sub>2</sub> cycle can still be thought of as being composed of two elementary Brayton cycles operated by  $m_1$  and  $m_2$ . The first cycle (Figure 6a) acts only partially as a topping cycle because it receives heat not only from the external heat source in the heater (at the upper temperature) but also from the second elementary cycle in the LTR (at the lower temperature). In addition, the second elementary cycle (Figure 6b) acts only partially as a bottoming cycle because, besides receiving heat from the first cycle in the HTR, it also provides heat to the latter in the LTR.

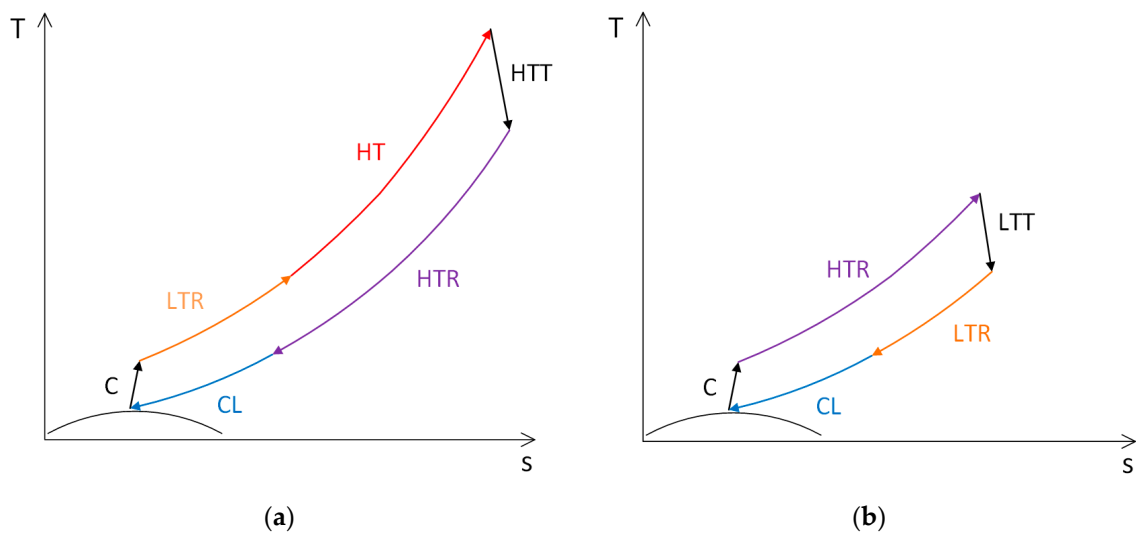


Figure 6. Decomposition of the dual recuperated s-CO<sub>2</sub> cycle into two elementary thermodynamic cycles: (a) First elementary cycle; (b) Second elementary cycle.

In Figure 6, the heat transfer from the first cycle to the second cycle is shown using a violet color, like in the previous cases, whereas the heat transfer from the second cycle to the first one is shown in orange. Both the HTR and the LTR are actually the plant components that enable the interaction between the two elementary cycles and do not act as traditional recuperators.

## 2.2. Modeling and Thermodynamic Optimization

The s-CO<sub>2</sub> power cycles were modeled in the Engineering Equation Solver (EES) environment using a consistent set of assumptions for a fair comparison. A thermodynamic optimization was performed to find the optimum parameters of each s-CO<sub>2</sub> power cycle layout for utilization of a waste heat source with an inlet temperature of 600 °C. The steady-state mass and energy balances for each plant component are not shown for brevity.

### 2.2.1. Objective Function and Other Performance Metrics

The aim of the thermodynamic optimization set up in this study was the maximization of the “total heat recovery efficiency” ( $\eta_{TOT}$ ), which is the ratio between the net power output ( $\dot{W}_{net}$ ) and the heat available from the waste heat source ( $\dot{Q}_{hs,av}$ ) from the inlet temperature ( $T_{in}$ ) to the ambient temperature ( $T_{amb}$ ):

$$\eta_{TOT} = \frac{\dot{W}_{net}}{\dot{Q}_{hs,av}} = \frac{\dot{W}_{net}}{\dot{m}_{hs} \cdot c_p \cdot (T_{in} - T_{amb})}. \quad (1)$$

In this study, the net power output of all layouts was set to equal 1 MW and the mass flow rate of the heat source ( $\dot{m}_{hs}$ ) was calculated accordingly. Thus, the maximization of the net power output from a given waste heat source translates to the minimization of the mass flow rate of the heat source required to generate such a fixed amount of power.

The total heat recovery efficiency can be interpreted as the product of two more elementary performance metrics, namely the “thermal efficiency” of the power cycle ( $\eta_{th}$ ) and the “heat recovery effectiveness” ( $\phi$ ) in the heat transfer process between the heat source and the power cycle:

$$\eta_{TOT} = \eta_{th} \cdot \phi. \quad (2)$$

Indeed,  $\eta_{th}$  is the ratio between the net power and the heat transferred from the heat source to the power cycle ( $\dot{Q}_{hs,in}$ ):

$$\eta_{th} = \frac{\dot{W}_{net}}{\dot{Q}_{hs,in}} = \frac{\dot{W}_{net}}{\dot{m}_{hs} \cdot c_p \cdot (T_{in} - T_{out})}, \quad (3)$$

whereas  $\phi$  is the ratio between the heat transferred to the power cycle and the heat available from the heat source from the inlet temperature to the ambient temperature:

$$\phi = \frac{\dot{Q}_{hs,in}}{\dot{Q}_{hs,av}} = \frac{(T_{in} - T_{out})}{(T_{in} - T_{amb})}. \quad (4)$$

From Equation (2), it is clearly apparent that both elementary performance metrics have the same weight in determining the final value of  $\eta_{TOT}$ . Thus, in the search of the maximum power output from a given heat source, it is important to maximize both of them. The improvement in  $\eta_{th}$  is obtained by increasing the average temperature of the heat input from the heat source and decreasing the average temperature of the heat rejection to the environment. Instead, the improvement in  $\phi$  is obtained by cooling down the heat source to the highest extent in the heat transfer process to the power cycle. These two requirements are generally antithetic because the cooling of the heat source in the heat transfer process implies heat input at lower temperatures. The target of the thermodynamic optimization is to identify those conditions (i.e., the values of the optimum decision variables), which represent a balance between high  $\eta_{th}$  and high  $\phi$  that yields the highest  $\eta_{TOT}$ .

While this approach based on the decomposition of the overall performance metric ( $\eta_{TOT}$ ) into two elementary sub-metrics (i.e.,  $\eta_{th}$ ,  $\phi$ ) has been widely applied in the field of organic Rankine cycles (see, e.g., [37]), it has been seldom used in the field of s-CO<sub>2</sub> power cycles and almost exclusively for the optimum point (see, e.g., Wright et al. [22]). Thus, one of the goals of this work was to apply this

approach, introduced in [36], to explore the potential of the advanced s-CO<sub>2</sub> power cycle layouts in both converting heat into power and extracting heat from the heat source. The response surfaces of  $\eta_{th}$ ,  $\phi$ , and  $\eta_{TOT}$  were explored in a wide range of decision variables to verify the flatness of the objective function in the neighborhood of the optimum and the main reasons behind the trend of  $\eta_{TOT}$ .

### 2.2.2. Decision Variables and Main Assumptions

The heat source is composed of flue gases having an inlet temperature of 600 °C and a specific heat typical of the exhausts from a gas turbine [38] or an internal combustion engine [39]. The assumption of a constant specific heat makes the application of the results obtained to different waste heat sources straightforward.

For each cycle layout, the decision variables in the optimization of  $\eta_{TOT}$  are the mass flow fraction ( $x$ ) in the splitter at the outlet of the compressor and the maximum cycle temperature ( $TIT$ ), shown within the green labels in Figures 1, 3 and 5. There are three other cycle parameters with a significant impact on the final performance, namely the maximum cycle pressure, limited to 20 MPa, and the minimum cycle pressure and temperature that were taken to equal 7.63 MPa and 32 °C, respectively, following [12,36].

Furthermore, the performance of the equipment (heat exchangers, turbomachinery, etc.) strongly affects the performance of the overall system and was set carefully to ultimately obtain a reliable performance prediction and comparison. Following the literature, the effectiveness of the recuperator/s was fixed at 95% (see, e.g., [7]). Shiferaw et al. [40] discussed the design features of printed circuit heat exchangers' (PCHEs) recuperators and the relationship between the effectiveness and cost in the search for an efficient power cycle and cost-effective design. They showed that a heat exchanger with an effectiveness of up to 95% provides a significant gain in cycle efficiency at a moderate cost. Also, the compact recuperator based on a different design based on the microchannel technology tested in [41] reached values of effectiveness of up to 97%.

The minimum temperature difference between the heat source and the CO<sub>2</sub> in the heater/s ( $\Delta T_{min}$ ) was fixed at 50 °C as suggested in the design of gas-to-gas heat exchangers [42]. The new heat exchanger between waste gases and supercritical CO<sub>2</sub> based on the plate-type design, rather than on the more common finned tube design, built and tested in [43] reached an effectiveness in the range 77%–87%, which is consistent with the assumed temperature difference assumed in this study.

The pressure losses in all heaters and recuperators were neglected for an easier comparison against other studies on s-CO<sub>2</sub> power cycles, or different waste heat-to-power technologies, where pressure losses are often neglected at the conceptual stage of the design. The reader is referred to a previous study of the first current author [36] for the impact of pressure losses on the performance of s-CO<sub>2</sub> power cycles.

The isentropic efficiencies of the compressor and turbine/s were fixed at 80% and 85%, respectively, taking into account both the small size of the system (which implies higher losses and lower efficiencies) and the recent advancements in the design of CO<sub>2</sub> turbomachinery. Cich et al. [44] report a design turbine efficiency of 85% and compressor efficiencies of 78% to 82% for a 10 MW recompression s-CO<sub>2</sub> cycle. A maximum total-to-static efficiency of about 70% was measured for a 50 kW radial compressor tested at Sandia National Laboratories [45], which, however, was designed starting from traditional design tools adjusted for the real gas behavior of CO<sub>2</sub>. Noall and Pasch [46] estimated a realistically achievable compressor isentropic efficiency of 83% to 85% for a 50 MW plant. The total-to-static efficiency of the 1.16 MW s-CO<sub>2</sub> turbine modelled in [47] was 85.4%, which is consistent with the size and efficiency of the present study. The partial heating layout includes a single larger CO<sub>2</sub> turbine rather than two smaller turbines, which is beneficial in terms of the turbine efficiency. However, a detailed evaluation of the turbine efficiency that considers the impact of the turbine architecture (radial, single axial, multistage axial, etc. [48]), size, and expansion ratio [49] is left to a further stage of the design process.

The thermodynamic properties of carbon dioxide were obtained using the equation of state developed by Span and Wagner [50], which is embedded in EES and provides an accurate calculation of the real gas behavior of CO<sub>2</sub> in a wide range of pressures and temperatures. The precise description of the thermodynamic properties, especially in the vicinity of the critical point ensured by [50], is crucial for the accurate analysis and performance prediction of the s-CO<sub>2</sub> power cycles. Table 1 summarizes all the main assumptions, which are consistent with [36], for a direct comparison with the traditional s-CO<sub>2</sub> power cycles.

**Table 1.** Main assumptions in the simulation models of s-CO<sub>2</sub> cycle layouts.

Parameter	Value
Heat source inlet temperature, $T_{in}$ (°C)	600
Heat source specific heat, $c_p$ (kJ/kg-K)	1.17
Ambient temperature, $T_{amb}$ (°C)	20
Compressor inlet pressure, $p_1$ (MPa)	7.63
Compressor inlet temperature, $T_1$ (°C)	32.0
Maximum cycle pressure, $p_2$ (MPa)	20.0
Recuperator/s effectiveness, $\varepsilon$ (%)	95.0
Minimum temperature difference in the heater/s, $\Delta T_{min}$ (°C)	50
Pressure drops in recuperators and heaters, $\Delta p$ (bar)	-
Isentropic efficiency turbine/s, $\eta_{is,T}$ (%)	85
Isentropic efficiency compressor, $\eta_{is,C}$ (%)	80
Mechanical/generator efficiency turbine/s, $\eta_{mg,T}$ (%)	95
Mechanical efficiency compressor, $\eta_{m,C}$ (%)	98

### 2.2.3. Thermal Efficiency of Elementary Thermodynamic Cycles

While the decomposition of s-CO<sub>2</sub> power cycles into elementary Brayton cycles is already meaningful at a qualitative level to understand the genesis of such advanced cycle layouts (see Section 2.1), further insights could be provided by a quantitative analysis that evaluates the thermal efficiency of each elementary cycle.

The thermal efficiency of the first elementary thermodynamic cycle (topping cycle) was calculated as:

$$\eta_{th,1} = \frac{\dot{W}_{net,1}}{\dot{Q}_{hs,1}}, \quad (5)$$

where  $\dot{W}_{net,1}$  is the net power generated by the mass flow rate,  $m_1$ , operating in the first elementary thermodynamic cycle and  $\dot{Q}_{hs,1}$  is the heat transferred from the external heat source to  $m_1$ .

Instead, the thermal efficiency of the second elementary thermodynamic cycle (bottoming cycle) is:

$$\eta_{th,2} = \frac{\dot{W}_{net,2}}{\dot{Q}_{rec,1 \rightarrow 2}}, \quad (6)$$

where  $\dot{W}_{net,2}$  is the net power generated by the mass flow rate,  $m_2$ , operating in the second elementary thermodynamic cycle, and  $\dot{Q}_{rec,1 \rightarrow 2}$  is the heat recovered from the exhaust of the first elementary cycle and transferred to  $m_2$ .

The analysis in Section 2.1 showed that the decomposition into a pure topping cycle and a pure bottoming cycle strictly applies only to the dual flow split with a dual expansion s-CO<sub>2</sub> power cycle. Nevertheless, the calculation of the thermal efficiencies of elementary cycles can still be theoretically carried out for the remaining layouts. In particular, the additional term  $\dot{Q}_{hs,2}$  was added at the denominator of Equation (6) to take into account the heat transferred from the external heat source to  $m_2$  in the partial heating layout. Instead, the heat transferred from cycle 2 to cycle 1 in the dual

recuperated layout (orange process in Figure 6) was not added at the denominator of Equation (5), being treated in the same way as a regenerative heat transfer.

The achievement of high thermal efficiencies in both elementary cycles is a prerequisite to reach a high  $\eta_{TOT}$ , but not sufficient. Indeed, it must be accompanied by a high heat recovery from the external heat source (which is quantified by  $\phi$ ) and a high heat recovery from the turbine exhausts of both elementary cycles. While the heat of the turbine exhaust of the first elementary cycle is recovered by the second elementary cycle, the heat of the turbine exhaust of the latter is recovered by internal regeneration within the elementary cycle itself (single flow split with dual expansion and partial heating layouts) or heat transfer back to the first elementary cycle (dual recuperated layout).

### 3. Results

#### 3.1. Single Flow Split with Dual Expansion $s$ -CO<sub>2</sub> Power Cycle

Figure 7 shows the variation of  $\eta_{TOT}$  for the single flow split with dual expansion cycle in a wide range of variation of the decision variables. The trend of variation of  $\eta_{th}$  (not shown for brevity) is the same as  $\eta_{TOT}$ , but its values are just scaled up by the reciprocal of  $\phi$ , with the latter being constant ( $\phi = 0.8377$ ) over the entire domain of the decision variables. The maximum  $\eta_{TOT}$  (22.3%) is obtained at the maximum  $TIT$  of 550 °C and  $x = 0.35$ . However, a region of high  $\eta_{TOT}$  occurs at  $TIT$  higher than 450 °C and  $x$  in the range 0.32–0.5 that is asymmetrical to the optimum. Note that a wider domain of  $x$  was considered compared to [36] to explore the rapid decay of  $\eta_{TOT}$  at low  $x$  values.

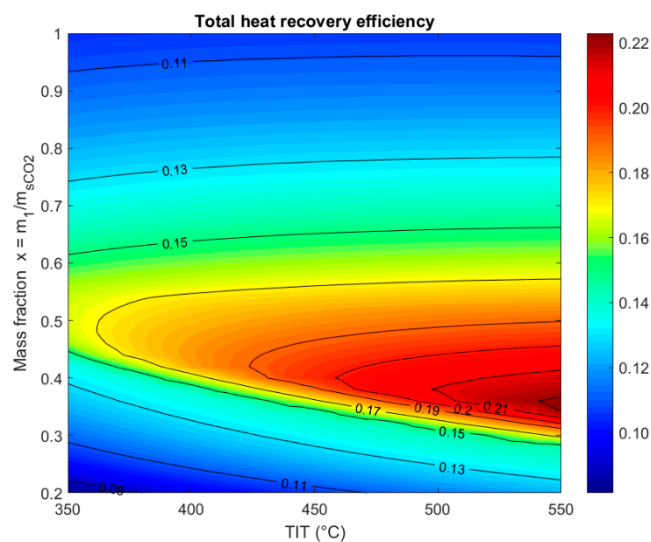


**Figure 7.** Variation of  $\eta_{TOT}$  with  $TIT$  and  $x$  for the single flow split with a dual expansion cycle.

Table 2 shows the values of the performance metrics and cycle parameters at the optimum point and at four sub-optimum points forming a parallelogram on the left of the optimum. At the optimum point, the temperature at the inlet of the LTT ( $T_7$ ) is moderately high, the temperatures of the two streams at the mixing point are similar ( $T_5 \approx T_8$ ), and the heat at the exhaust from both the HTT and the LTT is fully recovered (i.e.,  $T_{10} \rightarrow T_2$ ). However, it must be noted that the temperature at the inlet of the LTT is much lower than the temperature at the exhaust of the HTT ( $T_7 \ll T_4$ ) due to a mismatch between the mass flow rates and the thermal flow capacities in the HTR, inherent to this cycle layout.

**Table 2.** Performance metrics and cycle parameters at the optimum and four sub-optimum points for the single flow split with a dual expansion cycle. All temperatures are in °C.

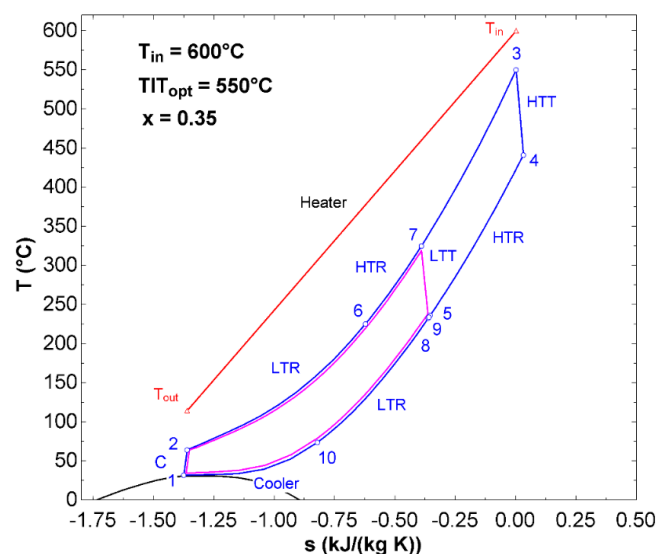
$TIT$	$x$	$\eta_{TOT}$	$\eta_{th}$	$\Phi$	$T_2$	$T_4$	$T_5$	$T_6$	$T_7$	$T_8$	$T_9$	$T_{10}$	$T_{out}$
550 <sup>1</sup>	0.35 <sup>1</sup>	22.30	26.62	83.77	64.1	441.4	236.2	225.4	324.9	232.7	233.9	73.8	114.1
500	0.30	14.18	16.93	83.77	64.1	395.3	80.7	64.1	131.9	55.3	62.1	62.1	114.1
500	0.50	18.76	22.39	83.77	64.1	395.3	274.5	268.2	379.2	283.3	278.9	124.6	114.1
400	0.40	16.33	19.50	83.77	64.1	302.6	106.2	95.9	178.3	95.5	99.7	65.9	114.1
400	0.60	15.76	18.82	83.77	64.1	302.6	244.1	221.4	298.6	208.0	229.7	128.0	114.1

<sup>1</sup> Optimum values of the decision variables.

If the mass flow fraction,  $x$ , is decreased from the optimum ( $x = 0.30$ ), the CO<sub>2</sub> temperature at the outlet of HTR and entering the LTT is markedly reduced. This results in a temperature at the outlet of LTT lower than the compressor outlet temperature ( $T_8 < T_2$ ) and the consequent exclusion of LTR. Conversely, if  $x$  is increased ( $x = 0.50$ ), the temperature at the inlet of LTT increases and approaches the temperature at the outlet of HTT ( $T_7 \rightarrow T_4$ ). On the other hand, the heat at the exhaust from both HTT and LTT is only partially recovered, as demonstrated by the high temperature at the inlet of the cooler ( $T_{10} > 120$  °C). The penalty in  $\eta_{th}$  and  $\eta_{TOT}$  deriving from the low  $x$  is much higher than that at the high  $x$ . Indeed, the slope of the response surface is much steeper for decrements of  $x$  from the optimum rather than for increments, as clearly shown by the distance between the contour lines at constant  $\eta_{TOT}$  in Figure 7.

The decrease of  $TIT$  ( $TIT = 400$  °C in Table 2) implies a contextual decrease of the maximum cycle temperature and inlet temperature to LTT, without involving any gain in heat extraction from the heat source. Thus, the overall effect is the decrease of  $\eta_{th}$  and  $\eta_{TOT}$ .

Figure 8 shows the  $T$ - $s$  diagram of the single flow split with a dual expansion cycle at the optimum point. The power cycle is actually composed of two partially superimposed Brayton cycles: The first elementary cycle (in blue) operates between the minimum and maximum temperatures and receives heat from the heat source; the second elementary cycle (in pink) recovers heat from the exhaust of the first cycle and therefore reaches a lower maximum temperature. Accordingly, the thermal efficiency of elementary topping cycle 1 is the ratio between the net power produced by the mass flow rate,  $m$ , and the heat input from the external heat source (as per Equation (5)). Instead, the thermal efficiency of the elementary bottoming cycle 2 is the ratio between the net power produced by  $m_2$  and the heat input from the exhaust of topping cycle 1 (as per Equation (6)).



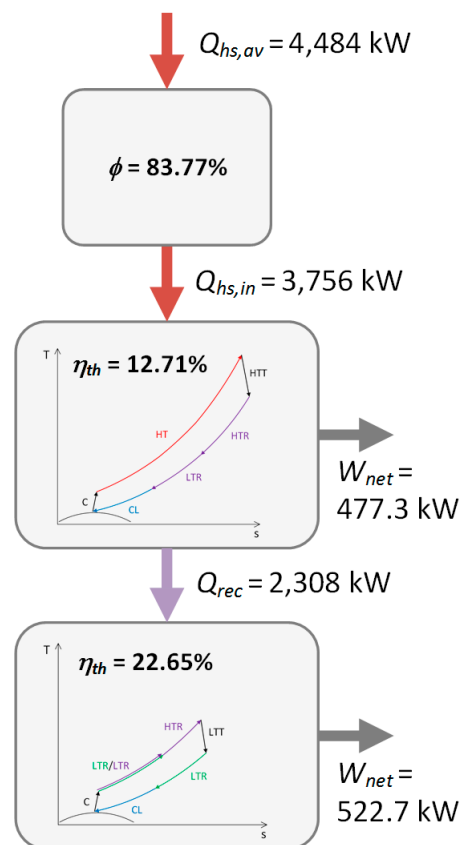
**Figure 8.** Single flow split with dual expansion layout:  $T$ - $s$  diagram of the optimum thermodynamic cycle maximizing  $\eta_{TOT}$ . The cooling profile of the heat source is superimposed.

Table 3 shows that despite the lower TIT, the thermal efficiency of elementary cycle 2 is almost 10% higher than that of elementary cycle 1 due to the recuperative layout. While the topping elementary cycle enables an effective heat extraction from the external heat source ( $\phi = 83.77\%$ ), the bottoming cycle enables an effective heat recovery from the exhaust of the high temperature CO<sub>2</sub> turbine.

**Table 3.** Thermal efficiency of the two elementary thermodynamic cycles that compose the single flow split with dual expansion s-CO<sub>2</sub> power cycle.

Parameter	Elementary Cycle 1 (Topping, Figure 2a)	Elementary Cycle 2 (Bottoming, Figure 2b)
Heat input from the external heat source (kW)	3756	-
Heat recovered from the exhaust of the first cycle (kW)	-	2308
Net power output (kW)	477.3	522.7
Thermal efficiency of elementary cycles (%)	12.71	22.65

Figure 9 shows that the net power output is the useful product of a chain of efficiencies, where the thermal efficiencies of the elementary thermodynamic cycles play a key role.



**Figure 9.** Single flow split with a dual expansion cycle. Breakdown of the overall performance into a chain of efficiencies, which include the thermal efficiencies of the elementary cycles.

### 3.2. Partial Heating s-CO<sub>2</sub> Power Cycle

The trend of the variation of  $\eta_{TOT}$  for the partial heating cycle in a wide range of TIT and  $x$  is shown in Figure 10a. The maximum  $\eta_{TOT}$  is obtained at a moderate TIT ( $=390$  °C) and low  $x$  ( $=0.30$ ). The lines at constant  $\eta_{TOT}$  form a series of non-regular rectangles around the optimum point, which implies a higher flatness of the objective function with TIT than with  $x$ . While the maximum  $\eta_{th}$  is achieved at the highest TIT and low  $x$  in the right low corner of Figure 10b, the maximum  $\phi$  is obtained

in the opposite corner in a wide region roughly above the bisector of Figure 10c. The trend of  $\eta_{TOT}$  is the product of the two opposed metrics according to Equation (2).

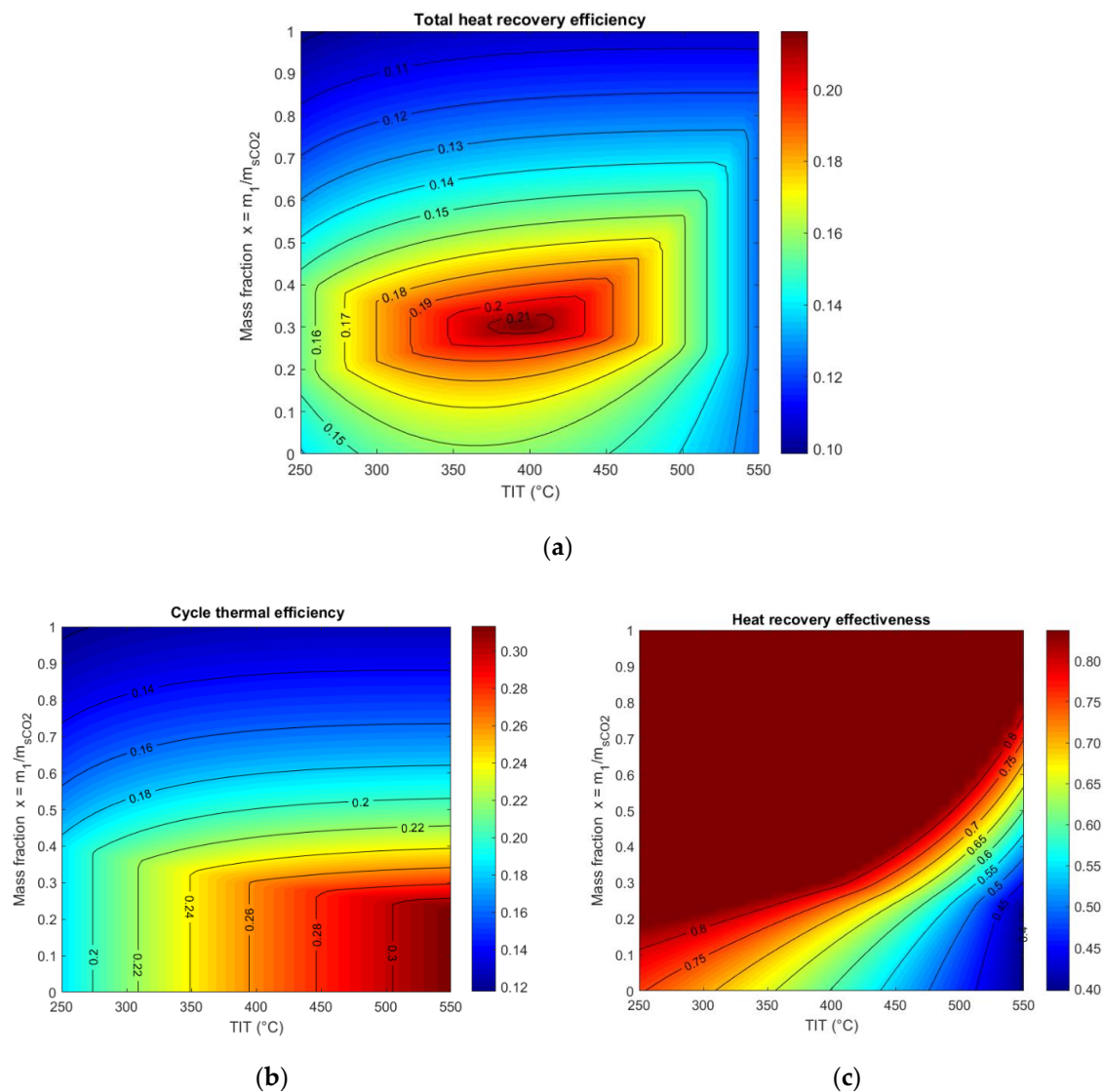


**Figure 10.** Variation of the performance metrics with TIT and  $x$  for the partial heating cycle: (a) Total heat recovery efficiency; (b) Cycle thermal efficiency; (c) Heat recovery effectiveness.

Table 4 shows the values of the performance metrics and cycle parameters at the optimum point and at four sub-optimum points forming a rhombus around the optimum.

**Table 4.** Performance metrics and cycle parameters at the optimum and four sub-optimum points for the partial heating cycle. All temperatures are in  $^{\circ}C$ .

TIT	$x$	$\eta_{TOT}$	$\eta_{th}$	$\phi$	$T_2$	$T_3$	$T_4$	$T_5$	$T_7$	$T_8$	$T_{inter}$	$T_{out}$
390 <sup>1</sup>	0.30 <sup>1</sup>	21.63	25.82	83.77	64.1	276.0	280.1	278.9	293.3	75.6	328.9	114.1
400	0.50	16.79	20.05	83.77	64.1	169.1	290.7	227.2	302.6	135.0	277.2	114.1
400	0.10	16.69	26.23	63.62	64.1	225.1	225.1	225.1	302.6	76.1	275.1	231.0
500	0.30	16.11	27.46	58.67	64.1	378.7	378.7	378.7	395.3	97.8	428.7	259.7
300	0.30	18.02	21.52	83.77	64.1	133.3	185.0	168.3	209.3	71.4	218.3	114.1

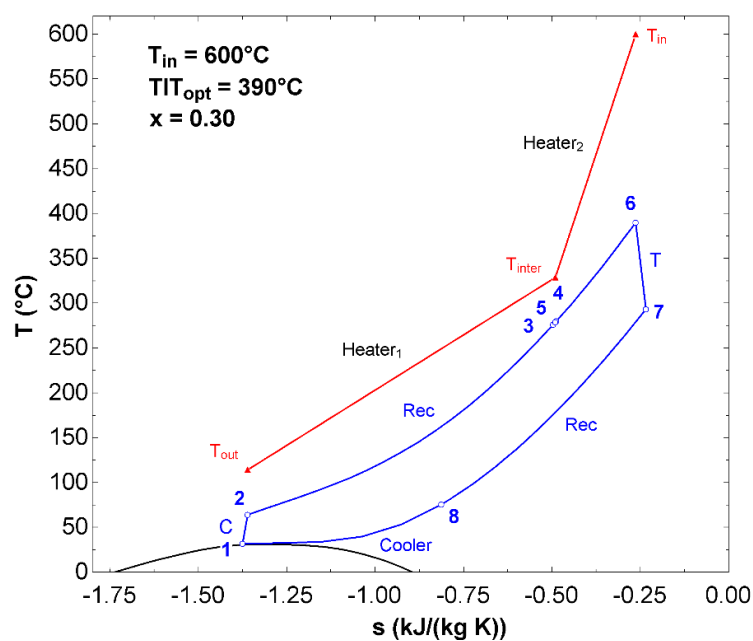
<sup>1</sup> Optimum values of the decision variables.

At the optimum  $\eta_{TOT}$ , the temperature of the two parallel branches entering the mixing point is almost equal (i.e.,  $T_3 \approx T_4$ ), the outlet temperature of the heat source is the minimum allowed, and the exhaust heat at the outlet of the CO<sub>2</sub> turbine is fully recovered ( $T_8 \rightarrow T_2$ ).

The increase of the mass flow fraction above the optimum point ( $x = 0.5$ ) results in a marked decrease of the outlet temperature in the upper branch ( $T_3$ ), a temperature mismatch at the mixing point ( $T_4 \gg T_3$ ), and the incomplete recovery of the turbine exhaust ( $T_8 \gg T_2$ ). On the other hand, the decrease of the mass flow fraction below the optimum point ( $x = 0.1$ ) implies an incomplete utilization of the external heat source, which leaves the plant at a temperature much higher than the minimum allowed. The former sub-optimum condition (high  $x$ ) results in a marked decrease of  $\eta_{th}$  and unvaried  $\phi$ , whereas the latter (low  $x$ ) results in a marked decrease of  $\phi$  and almost unvaried  $\eta_{th}$ .

The increase of  $TIT$  above the optimum point (e.g., 500 °C in Table 4) implies a marked increase of the CO<sub>2</sub> temperature at the inlet of heater 2 ( $T_5$ ) and the incomplete utilization of the external heat source. In addition, the exhaust temperature at the outlet of the recuperator ( $T_8$ ) turns out to be higher than the minimum. Thus, the moderate improvement in  $\eta_{th}$  is totally overcome by the marked decrease in  $\phi$ . Instead, a decrease of  $TIT$  below the optimum (e.g., 300 °C) results in a poor  $\eta_{th}$  dictated by the low maximum cycle temperature.

Figure 11 shows the  $T$ - $s$  diagram of the partial heating cycle at the optimum point. The power cycle is actually composed of two superimposed Brayton cycles operating between the same minimum and maximum temperatures. The thermal efficiency of the first elementary cycle (Figure 4a) is the ratio between the net power output obtained by the mass flow rate,  $m_1$ , and heat input from the external heat source in heaters 1 and 2 needed to heat CO<sub>2</sub> from the compressor outlet to the turbine inlet (as per Equation (5)). The thermal efficiency of the second elementary cycle (Figure 4b) is the ratio between the net power output obtained by  $m_2$  and the sum of the heat recovered from the exhaust of elementary cycle 1 and heat input from the external heat source in heater 2, (i.e., the term  $Q_{hs,2}$  in Equation 6 is added). The thermal efficiency of elementary cycle 2 is approximately two times higher than that of elementary cycle 1 due to the recuperated layout (Table 5). The elementary cycle 1 enables an effective heat extraction from the heat source ( $\phi = 83.77\%$ ), whereas the elementary cycle 2 enables an effective heat recovery from the exhaust of the CO<sub>2</sub> turbine.

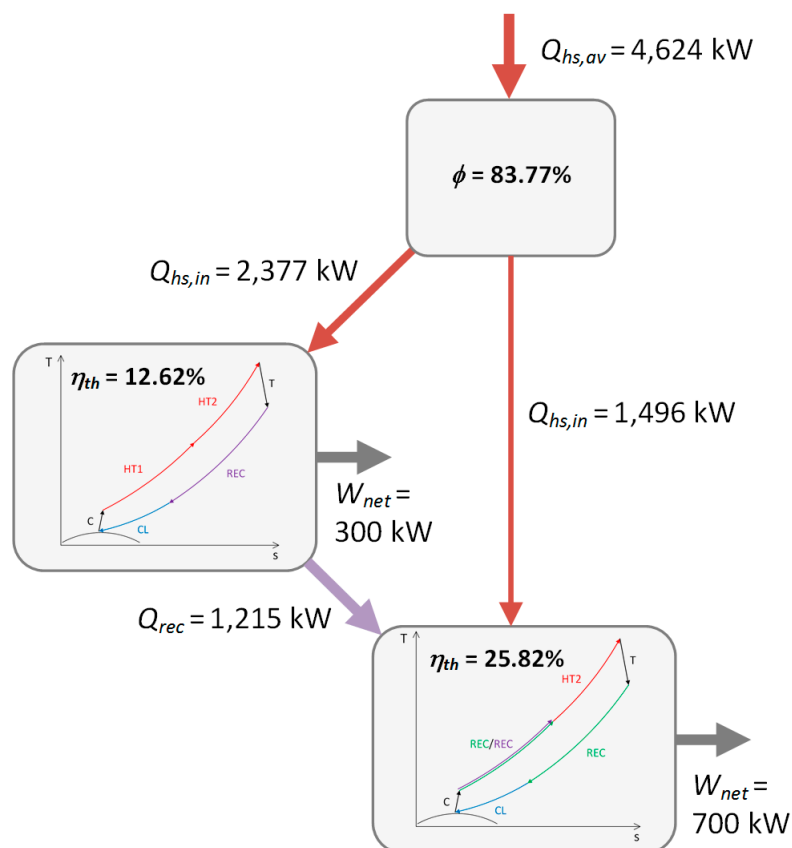


**Figure 11.** Partial heating layout:  $T$ - $s$  diagram of the optimum thermodynamic cycle maximizing  $\eta_{TOT}$ . The cooling profile of the heat source is superimposed.

**Table 5.** Thermal efficiency of the two elementary thermodynamic cycles that compose the partial heating s-CO<sub>2</sub> power cycle.

Parameter	Elementary Cycle 1 (Figure 4a)	Elementary Cycle 2 (Figure 4b)
Heat input from the external heat source (kW)	2377	1496
Heat recovered from the exhaust of the first cycle (kW)	-	1215
Net power output (kW)	300	700
Thermal efficiency of elementary cycles (%)	12.62	25.82

Figure 12 shows that the net power output is the useful product of a chain of efficiencies. The heat input from the external heat source is shared between the first and second elementary cycles. While the heat input to the first cycle produces power twice (in its original form in the first cycle and in a degraded form, degraded in temperature and amount, in the second thermodynamic cycle), the heat input to the second cycle produces power once. The thermal efficiency of the second elementary cycle in the partial heating layout cannot be directly compared against the corresponding efficiency in the single flow split with the dual expansion layout because the former benefits from the higher quality heat input.

**Figure 12.** Partial heating cycle. Breakdown of the overall performance into a chain of efficiencies, which include the thermal efficiencies of the elementary cycles.

### 3.3. Dual Recuperated s-CO<sub>2</sub> Power Cycle

The trend of the variation of  $\eta_{TOT}$  for the dual recuperated cycle in a wide range of  $TIT$  and  $x$  is shown in Figure 13a. The maximum  $\eta_{TOT}$  is obtained at a  $TIT = 520 \text{ }^\circ\text{C}$ , which is lower than the maximum temperature, and at  $x = 0.56$ . A region of high  $\eta_{TOT}$  is attained in a rather wide range of  $TIT$  between  $450$  and  $550 \text{ }^\circ\text{C}$  and a narrow interval of the mass flow fraction  $x$  between  $0.50$  and  $0.60$ . It is

interesting to note that the region of the highest  $\eta_{th}$  (Figure 13b) roughly corresponds to the region of the lowest  $\phi$  (Figure 13c), which still remains above 65.5%. The overall effect is the extension of the high  $\eta_{TOT}$  region to wider intervals of  $TIT$  and  $x$  than those maximizing  $\eta_{th}$ .

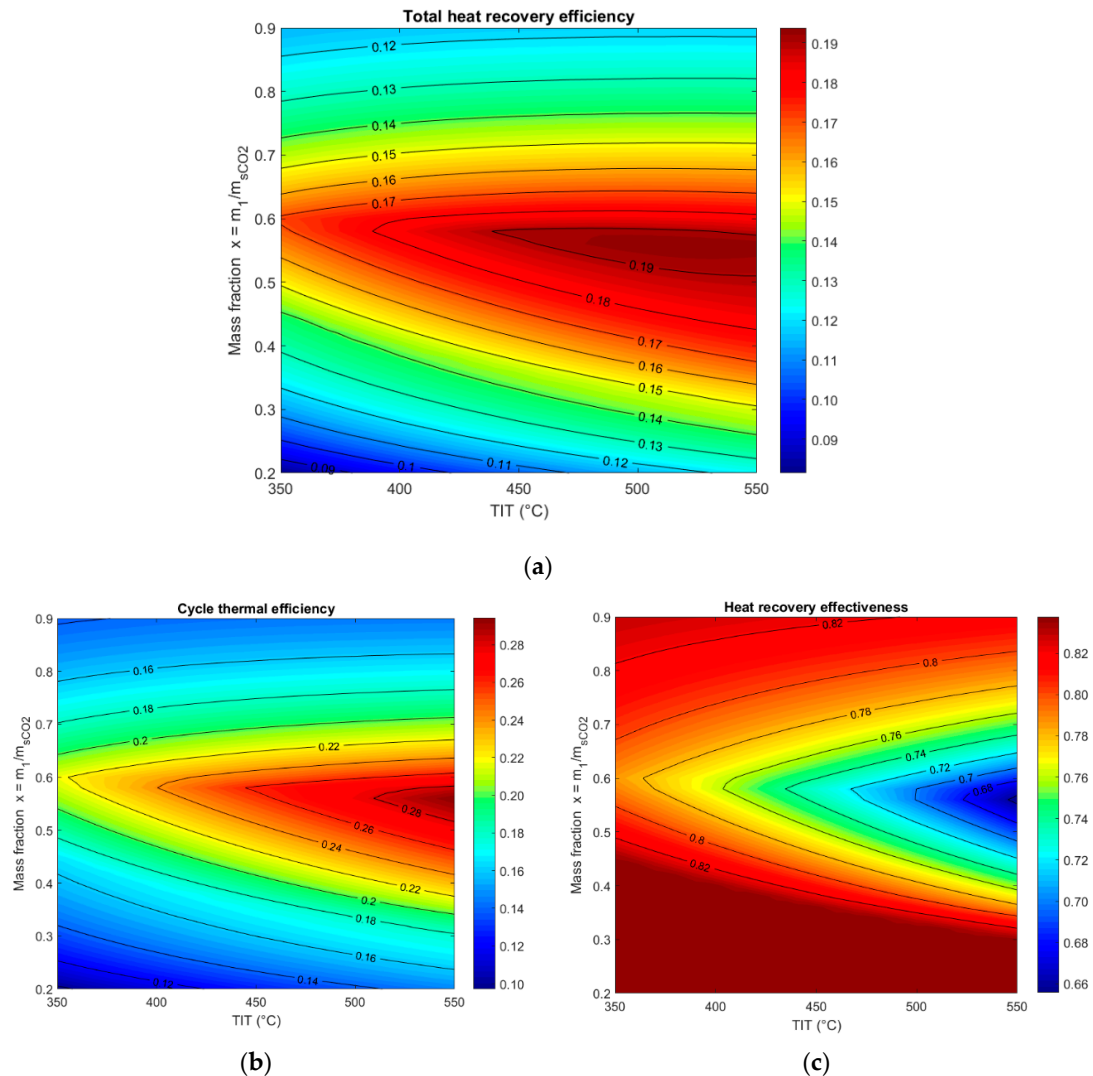


**Figure 13.** Variation of the performance metrics with TIT and  $x$  for the dual recuperated cycle: (a) Total heat recovery efficiency; (b) cycle thermal efficiency; (c) heat recovery effectiveness.

Table 6 shows the values of the performance metrics and cycle parameters at the optimum point and at four sub-optimum points forming a rectangle just to the left of the optimum.

**Table 6.** Performance metrics and cycle parameters at the optimum and four sub-optimum points for the dual recuperated cycle. All temperatures are in °C.

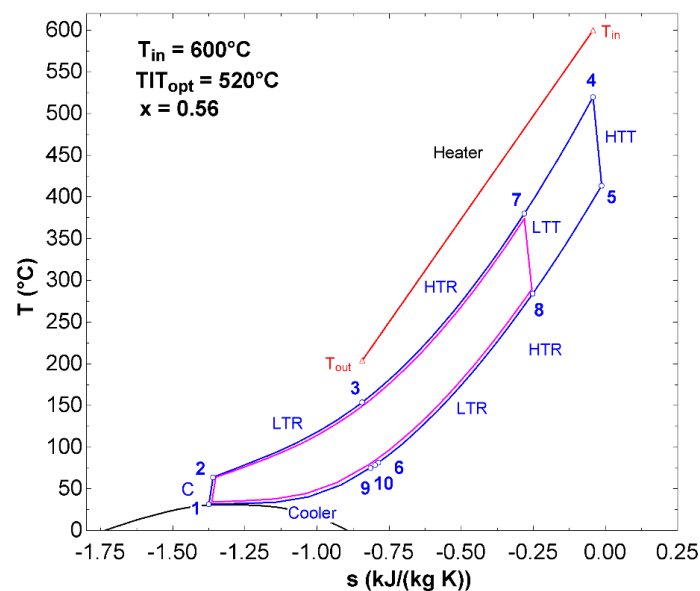
$TIT$	$x$	$\eta_{TOT}$	$\eta_{th}$	$\phi$	$T_2$	$T_3$	$T_5$	$T_6$	$T_7$	$T_8$	$T_9$	$T_{10}$	$T_{out}$
520 <sup>1</sup>	0.56 <sup>1</sup>	19.39	28.40	68.27	64.1	154.0	413.7	81.6	380.4	284.4	75.2	78.7	204
500	0.40	16.77	21.38	78.43	64.1	95.1	395.3	80.7	186.7	103.2	66.1	71.7	145.1
500	0.70	15.45	20.20	76.51	64.1	106.3	395.3	210.3	378.7	282.8	75.1	166.8	156.3
400	0.40	14.26	17.05	83.63	64.1	65.0	302.6	76.1	143.9	65.0	64.2	68.8	115.0
400	0.70	15.07	19.03	79.20	64.1	90.7	302.6	158.2	290.7	200.6	71.0	129.8	140.7

<sup>1</sup> Optimum values of the decision variables.

At the optimum point, the temperature increase of CO<sub>2</sub> in LTR is moderate (i.e.,  $T_8 \gg T_3$ ) so that a major fraction of the heat available from the external heat source can be recovered by the power cycle. Conversely, the temperature of the CO<sub>2</sub> stream at the outlet of HTR and entering the LTT is high and close to the exhaust temperature from the HTT (i.e.,  $T_7 \rightarrow T_5$ ). The heat at the outlet of both HTT and LTT is fully recovered and the temperatures of the streams entering the mixing point are close to the compressor outlet temperature ( $T_6, T_9, T_{10} \rightarrow T_2$ ). The high  $\eta_{th}$  is partially abated by the poor  $\phi$  but finally results in the highest  $\eta_{TOT}$ .

A reduction of  $x$  from the optimum ( $x = 0.40$ ) implies a significant reduction of the CO<sub>2</sub> temperature at the outlet of HTR and that entering the LTT. This, in turn, results in a decrease of the CO<sub>2</sub> temperature entering the heater. The marked reduction of  $\eta_{th}$  prevails on the moderate improvement of  $\phi$  and finally results in a reduction of  $\eta_{TOT}$ . These effects are even exacerbated by the reduction of  $TIT$  (e.g.,  $TIT = 400$  °C) that may even require the exclusion of LTR due to the low temperature at the LTT outlet ( $T_8 \approx T_2$ ). An increase of  $x$  ( $x = 0.70$ ) results in an incomplete recovery of the exhaust heat at the outlet of the HTT ( $T_6 \gg T_2$ ) to the detriment of  $\eta_{th}$ . The reduction of  $\eta_{th}$  is more pronounced in the presence of a lower  $TIT$  in spite of the lower CO<sub>2</sub> temperature at the inlet of the cooler.

Figure 14 shows the  $T$ - $s$  diagram of the dual recuperated cycle at the optimum point. The power cycle is actually composed of two partially superimposed Brayton cycles: The first elementary cycle (in blue) operates between the minimum and maximum temperature and mainly receives heat from the external heat source, and the second elementary cycle (in pink) recovers heat from the exhaust of the first cycle and therefore reaches a lower maximum temperature. Accordingly, the thermal efficiency of the first elementary cycle is the ratio between the net power output obtained by  $m_1$  and the heat input from the external heat source (as per Equation (5)). Instead, the thermal efficiency of the second elementary cycle is the ratio between the net power output obtained by the mass flow rate,  $m_2$ , and the heat recovered from the exhaust of the first elementary cycle (according to Equation (6)).



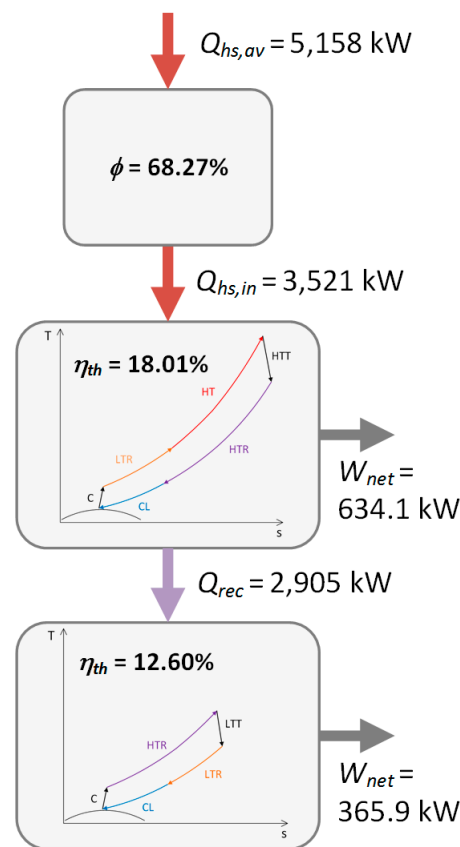
**Figure 14.** Dual recuperated layout:  $T$ - $s$  diagram of the optimum thermodynamic cycle maximizing  $\eta_{TOT}$ . The cooling profile of the heat source is superimposed.

Table 7 shows that the thermal efficiency of the first elementary cycle is higher than the corresponding cycles in the previous layouts due to CO<sub>2</sub> preheating by heat regeneration (orange process in Figure 6). The first elementary cycle enables a moderate heat extraction from the heat source ( $\phi = 68.27$ ), whereas the second elementary cycle enables an effective heat recovery from the exhaust of the higher temperature CO<sub>2</sub> turbine.

**Table 7.** Thermal efficiency of the two elementary thermodynamic cycles that compose the dual recuperated s-CO<sub>2</sub> power cycle.

Parameter	Elementary Cycle 1 (Figure 6a)	Elementary Cycle 2 (Figure 6b)
Heat input from the external heat source (kW)	3521	-
Heat recovered from the exhaust of cycle 1 (kW)	-	2905
Net power output (kW)	634.1	365.9
Thermal efficiency of elementary cycles (%)	18.01	12.60

Figure 15 shows that the net power output is the useful product of a chain of efficiencies, where the thermal efficiencies of the elementary thermodynamic cycles play a key role.



**Figure 15.** Dual recuperated cycle. Breakdown of the overall performance into a chain of efficiencies, which include the thermal efficiencies of the elementary cycles.

### 3.4. Performance Comparison

Table 8 shows the optimum values of the decision variables and performance metrics for the three s-CO<sub>2</sub> cycles considered in this work obtained for a  $T_{in}$  equal to 600 °C. The last column includes the optimum values obtained for the traditional single recuperated s-CO<sub>2</sub> cycle, used as the baseline (see [36]). Among the novel layouts, the highest  $\eta_{TOT}$  is achieved by the single flow split with a dual expansion cycle, and the lowest by the dual recuperated cycle. Both the single flow split with dual expansion and the partial heating cycles reach the highest  $\phi$  (dictated by the compressor outlet temperature and  $\Delta T_{min}$  in the heater), but the  $\eta_{th}$  of the former is 0.8% higher than that of the latter. The dual recuperated cycle shows the lowest  $\phi$  but the highest  $\eta_{th}$ .

**Table 8.** Optimum values of the decision variables and performance metrics for the three novel s-CO<sub>2</sub> cycles considered in this study compared to those of the single recuperated cycle used as the baseline.

Parameter	Single Flow Split with Dual Expansion	Partial Heating	Dual Recuperated	Single Recuperated
$T_{in}$ (°C)	600	600	600	600
$x$	0.35	0.30	0.56	-
$TIT$ (°C)	550	390	520	370
$\eta_{th}$	26.62	25.82	28.40	24.96
$\phi$	83.77	83.77	68.27	63.40
$\eta_{TOT}$	22.30	21.63	19.39	15.83

The optimum  $TIT$  of the single flow split with dual expansion is the highest allowed, whereas the optimum  $TIT$  of the partial heating cycle is 210 °C lower than  $T_{in}$ . The optimum  $TIT$  of the dual recuperated cycle deviates from the maximum by a few tens of degrees. The optimum mass fraction,  $x$ , is the highest in the dual recuperated cycle, whereas it is in the range 30%–35% for the other two cycles. All three novel s-CO<sub>2</sub> cycles outperform the baseline single recuperated cycle, both in terms of  $\eta_{th}$  and  $\phi$ , providing an incremental power of 22.5% to 40.9% in the utilization of the same waste heat source at 600 °C.

### 3.5. Exergy-Based Performance Comparison

Table 9 shows the results of the exergy analysis of the three novel s-CO<sub>2</sub> power cycles at the thermodynamic optimum. The highest exergy efficiency is reached by the single flow split with a dual expansion cycle and approaches 50%. The exergy efficiency of the partial heating cycle is only 1.5% lower than the maximum, whereas the penalty is 6.5% for the dual recuperated cycle. The exergy of the waste heat source required to generate the same fixed amount of electric power (1 MW) is 2 to 2.3 MW, with the overall exergy destructions/losses being in the range 1–1.3 MW depending on the cycle layout.

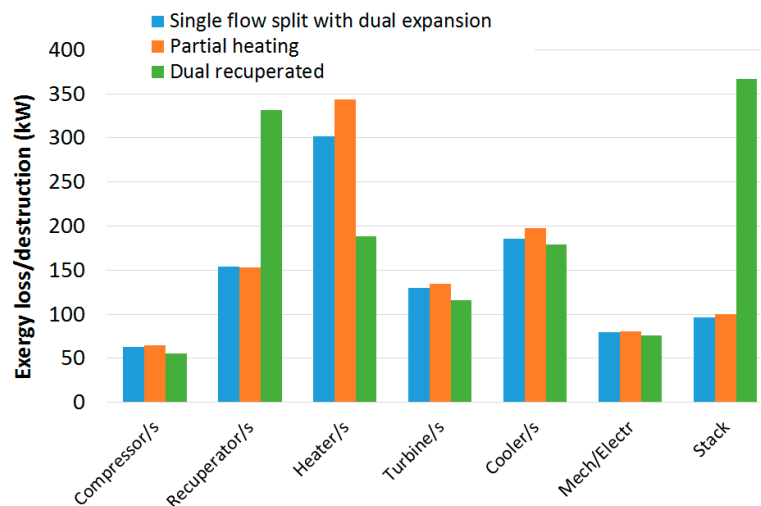
**Table 9.** Exergy of the waste heat source, net power output, and exergy efficiency of the three advanced s-CO<sub>2</sub> power cycles for WHR.

	Single Flow Split with Dual Expansion	Partial Heating	Dual Recuperated
Waste heat source (kW)	2010	2073	2312
Net power (kW)	1000	1000	1000
Total exergy destruction/loss (kW)	1010	1073	1312
Exergy efficiency (%)	49.75	48.24	43.24

The breakdown of the overall exergy destruction/loss into exergy losses occurring in the separate pieces of plant equipment is important to identify the source of these losses and understand any limitation of the s-CO<sub>2</sub> power cycle layouts. It can be easily seen from Table 10 and Figure 16 that the slight penalty in exergy efficiency of the partial heating cycle compared to the best cycle is mainly due to the higher exergy losses in the heaters. On the other hand, the penalty in exergy efficiency of the dual recuperated cycle is due to the relevant exergy loss in the stack and the exergy destruction in the recuperators.

**Table 10.** Breakdown of the exergy losses/destructions for the three advanced s-CO<sub>2</sub> power cycles for WHR. All values are in kW.

	Single Flow Split with Dual Expansion	Partial Heating	Dual Recuperated
Compressor	63.1	64.8	55.3
Recuperator	153.7 67.4(HTR)/86.3(LTR)	153.3	331.4 164.7(HTR)/166.7(LTR)
Heater	302.0	343.3 166(HEATER1)/ 177.3(HEATER2)	188.6
Turbine	130.0 46.8(HTT)/83.2(LTT)	134.3	115.7 65.5(HTT)/50.3(LTT)
Cooler	185.6	197.5	178.7
Mixer	0.03	0.04	0.24
Mech/Electr	79.5	80.2	76.1
Stack	96.7	99.7	366.5
Total	1010	1073	1312

**Figure 16.** Exergy losses/destructions in plant components for the s-CO<sub>2</sub> power cycles: Single flow split with dual expansion (blue bars), partial heating (orange), and dual recuperated (green).

The thermal profiles in the heaters (Figure 17) of the three s-CO<sub>2</sub> power cycles contain the information about the exergy destruction in the heat transfer between the external heat source and the high-pressure supercritical CO<sub>2</sub> and about the exergy loss in the stack. The dual recuperated cycle shows the minimum average temperature difference between supercritical CO<sub>2</sub> and waste heat source, which, however, leave the heater at the highest temperature (Figure 17c). The high specific heat of the high-pressure supercritical CO<sub>2</sub> at temperatures lower than 150 °C implies an increase of the temperature difference within the heater of the single flow split with a dual expansion cycle compared to the minimum of 50 °C reached at the two ends (Figure 17a). In the partial heating cycle, the staging of the heater improves the thermal match at lower temperatures (heater 1), but the moderate optimum turbine inlet temperature implies a divergence of the two thermal profiles at higher temperatures (heater 2) (Figure 17b).

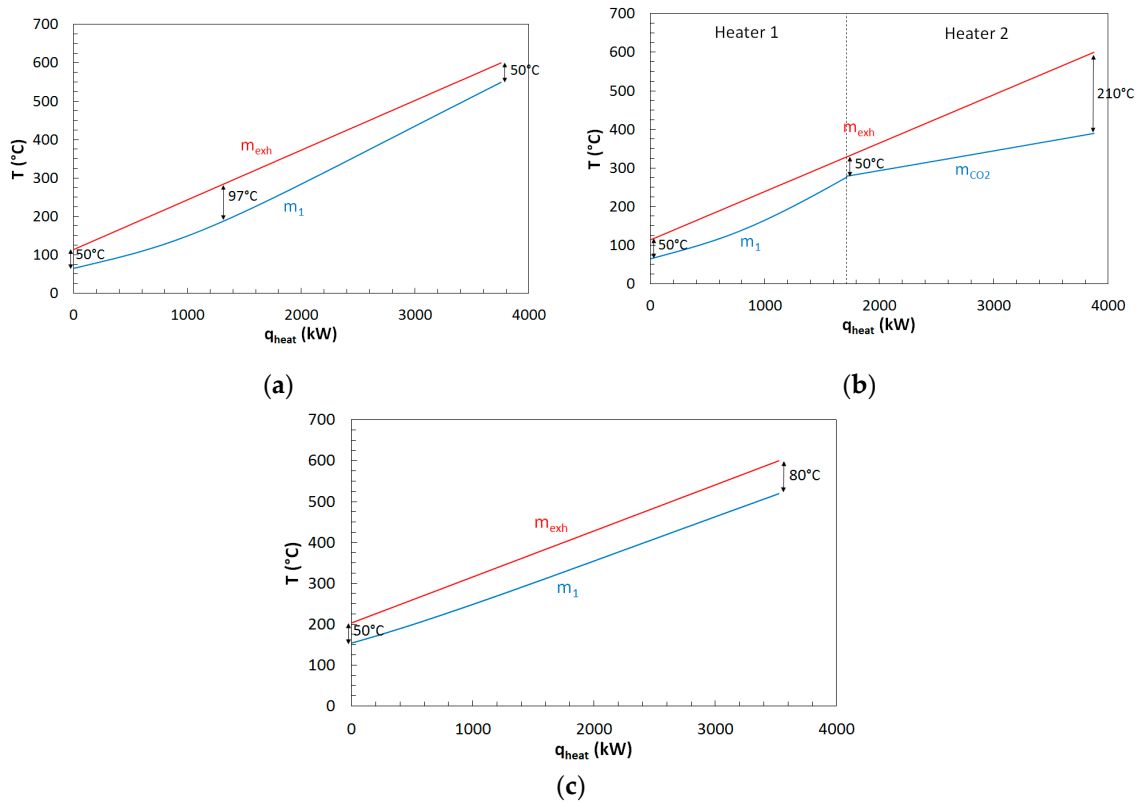


**Figure 17.** Temperature–heat load diagram in the heater/s of the s-CO<sub>2</sub> power cycles: (a) Single flow split with dual expansion; (b) partial heating; (c) dual recuperated.

The thermal profiles in the recuperators are shown in Figure 18. There is a high mismatch in both recuperators of the dual recuperated cycle due to the difference in the heat capacity flowrates between the hot and cold side, which is more pronounced in the LTR (Figure 18c). The thermal match is improved in the recuperator of the partial heating cycle (Figure 18b) and in the LTR of the single flow split with a dual expansion cycle (Figure 18a), where the entire mass flow rate of CO<sub>2</sub> on the hot side compensates for the lower specific heat. It is noteworthy that in all layouts, the heat of CO<sub>2</sub> at the turbine/s exhaust is completely recovered so that the exergy loss in the cooler is minimized. This demonstrates that the heat recovery from the waste heat source at low temperatures does not jeopardize the internal (regenerative) heat transfer and, ultimately, the thermal efficiency of these advanced cycles.

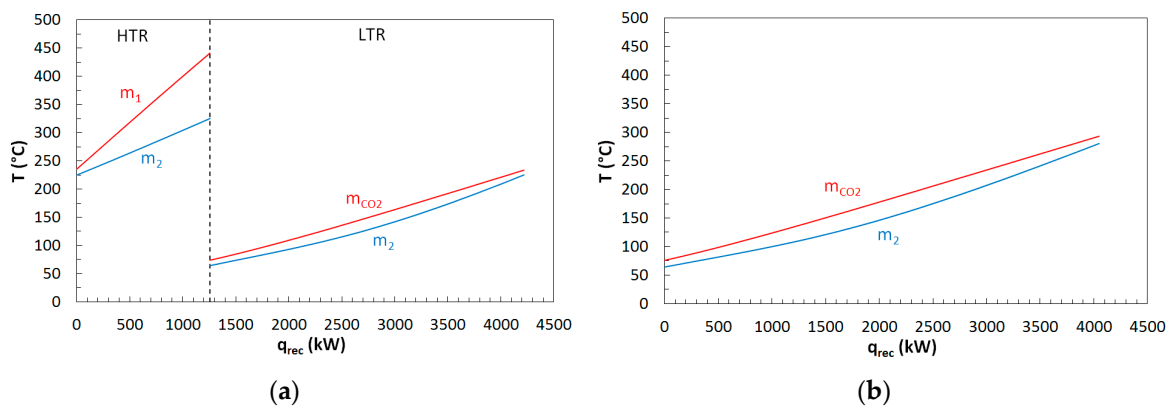


**Figure 18.** Cont.

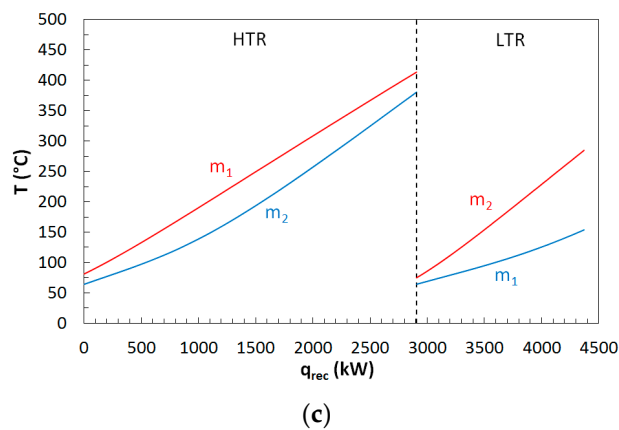


**Figure 18.** Temperature heat–load diagrams of the heat transfer between hot and cold CO<sub>2</sub> in the recuperator/s of the s-CO<sub>2</sub> power cycles: (a) Single flow split with dual expansion; (b) partial heating; (c) dual recuperated.

#### 4. Discussion

This work shows that the most promising novel configurations of advanced s-CO<sub>2</sub> power cycle layouts proposed in the recent literature can be simply generated by the combination of two elementary Brayton cycles, which are superimposed (i.e., joined) at lower temperatures but physically separated at higher temperatures. The distinct features of a topping and bottoming elementary cycle were strictly identified only in the single flow split with a dual expansion s-CO<sub>2</sub> power cycle, whereas the elementary cycles in the remaining layouts hold some peculiar aspects; hence, they are simply called the “first” and “second” elementary cycle. All three power cycles share the basic idea of cascade utilization of the waste heat that produces power twice, namely, in the first and second cycles. This idea is strictly implemented in the single flow split with dual expansion cycle, where the waste heat is entirely recovered and converted into power in the topping non-recuperated cycle, whose exhaust is, in turn, fully recovered and converted into power by the bottoming recuperated cycle. This strategy is relaxed in the partial heating s-CO<sub>2</sub> power cycle, where a fraction of waste heat produces power only once in the second cycle, though to the advantage of a higher thermal efficiency of the latter. Instead, it is even exacerbated in the dual recuperated layout, where a fraction of the exhaust heat from the second cycle substitutes for a fraction of the waste heat, yet to the detriment of heat extraction from the waste heat source.

The results obtained from the thermodynamic optimization show that the single flow split with a dual expansion cycle attains the highest total heat recovery efficiency, which reaches the remarkable value of 22.3% for WHR from waste gas at 600 °C, also considering the moderate size of the system. The net power output attainable by the single flow split with the dual expansion layout is 3.1% higher than the partial heating layout, 15% higher than the dual recuperated layout, and 40.9% higher than the single recuperated layout used as the baseline. For the best layout, the analysis of the objective function around the optimum showed that the region of the highest power output is obtained in a quite narrow range of turbine inlet temperatures approaching the maximum (550 °C). Indeed, a reduction of the inlet temperature from 550 to 400 °C implies a net loss of 4% in the total heat recovery efficiency. Instead, the region of the highest performance for the partial heating layout occurs in a wider range of temperatures centered on a much lower value around 390 to 400 °C compared to the other layouts. The high thermodynamic performance, which is only slightly lower than that attainable by the best layout, the moderate optimum cycle maximum temperatures, and the lowest number of components certainly place the partial heating cycle in a leading position for the recovery of high temperature waste heat. Finally, the traditional single recuperated layout shows all its limitations in WHR applications.

**Author Contributions:** Original draft preparation, G.M.; Review and editing, M.C. All authors have read and agreed to the published version of the manuscript.

**Funding:** This research was partially supported by the Fundação para a Ciência e a Tecnologia (FCT) through IDMEC, under LAETA, project UID/EMS/50022/2013.

**Conflicts of Interest:** The authors declare no conflict of interest. The funders had no role in the design of the study; in the collection, analyses, or interpretation of data; in the writing of the manuscript, or in the decision to publish the results.

## Nomenclature

### Acronyms

C	Compressor
CL	Cooler
LT	Low temperature
LTR	Low temperature recuperator
LTT	Low temperature turbine
HT	Heater or high temperature
HTR	High temperature recuperator
HTT	High temperature turbine
REC	Recuperator
sCO <sub>2</sub>	Supercritical CO <sub>2</sub>
s-CO <sub>2</sub>	Supercritical CO <sub>2</sub>
T	Turbine
TIT	Turbine inlet temperature
WHR	Waste heat recovery

### Parameters/Variables

$c_p$	specific heat, kJ/kg-K
$m$	mass flow rate, kg/s
$\dot{m}$	mass flow rate, kg/s
$p$	pressure, MPa
$\dot{Q}$	heat transfer rate, kW
$s$	specific entropy, kJ/kg-K
$x$	mass fraction
$T$	temperature, °C
$W$	power, kW
$\dot{W}$	power, kW
$\Delta$	difference
$\varepsilon$	recuperator effectiveness
$\eta$	efficiency, %
$\phi$	heat recovery effectiveness

### Subscripts

amb	ambient
av	available
C	compressor
hs	heat source
in	inlet
inter	intermediate
is	isentropic
m	mechanical
mg	mechanical/generator
min	minimum
net	net
opt	optimum
out	outlet
rec	recovered

T	turbine
th	thermal
TOT	total

## References

- Forman, C.; Muritala, I.K.; Pardemann, R.; Meyer, B. Estimating the global waste heat potential. *Renew. Sustain. Energy Rev.* **2016**, *57*, 1568–1579. [[CrossRef](#)]
- Papapetrou, M.; Kosmadakis, G.; Cipollina, A.; La Commare, U.; Micale, G. Industrial waste heat: Estimation of the technically available resource in the EU per industrial sector, temperature level and country. *Appl. Therm. Eng.* **2018**, *138*, 207–216. [[CrossRef](#)]
- Vance, D.; Nimbalkar, S.; Thekdi, A.; Armstrong, K.; Wenning, T.; Cresko, J.; Jin, M. Estimation of and barriers to waste heat recovery from harsh environments in industrial processes. *J. Clean. Prod.* **2019**, *222*, 539–549. [[CrossRef](#)]
- Firth, A.; Zhang, B.; Yang, A. Quantification of global waste heat and its environmental effects. *Appl. Energy* **2019**, *235*, 1314–1334. [[CrossRef](#)]
- Feher, E.G. The supercritical thermodynamic power cycle. *Energy Convers.* **1968**, *8*, 85–90. [[CrossRef](#)]
- Angelino, G. Carbon dioxide condensation cycles for power production. *J. Eng. Power-Trans. AAME* **1968**, *90*, 287–295. [[CrossRef](#)]
- Dostal, V.; Driscoll, M.J.; Hejzlar, P.A. *A Supercritical Carbon Dioxide Cycle for Next Generation Nuclear Reactors*; Massachusetts Institute of Technology: Cambridge, MA, USA, 2004.
- Mohagheghi, M.; Kapat, J. Thermodynamic optimization of recuperated s-CO<sub>2</sub> Brayton cycles for waste heat recovery applications. In Proceedings of the 4th International Symposium on Supercritical CO<sub>2</sub> Power Cycles, Pittsburgh, PA, USA, 9–10 September 2014.
- Khadse, A.; Blanchette, L.; Kapat, J.; Vasu, S.; Ahmed, K. Optimization of supercritical CO<sub>2</sub> Brayton cycle for simple cycle gas turbines exhaust heat recovery using genetic algorithm. In Proceedings of the ASME Turbo Expo 2017: Turbomachinery Tech. Conf. and Exposition, Article No. 63696, Charlotte, NC, USA, 26–30 June 2017.
- Moroz, L.; Pagur, P.; Rudenko, O.; Burlaka, M.; Joly, C. Evaluation for scalability of a combined cycle using gas and bottoming sCO<sub>2</sub> turbines. In Proceedings of the ASME Power & Energy, San Diego, CA, USA, 28 June–2 July 2015.
- Martínez, G.S.; Sánchez, D.; Crespi, F.; Gavagnin, G. A global approach to assessing the potential of combined cycles using supercritical technology. In Proceedings of the 1st Global Power and Propulsion Forum (GPPF), Zurich, Switzerland, 16–18 January 2017.
- Manente, G.; Lazzaretto, A. Innovative biomass to power conversion systems based on cascaded supercritical CO<sub>2</sub> Brayton cycles. *Biomass Bioenergy* **2014**, *69*, 155–168. [[CrossRef](#)]
- Hou, S.; Wu, Y.; Zhou, Y.; Yu, L. Performance analysis of the combined supercritical CO<sub>2</sub> recompression and recuperated cycle used in waste heat recovery of marine gas turbine. *Energy Convers. Manag.* **2017**, *151*, 73–85. [[CrossRef](#)]
- Zhang, Q.; Ogren, R.M.; Kong, S.-C. Thermo-economic analysis and multi-objective optimization of a novel waste heat recovery system with a transcritical CO<sub>2</sub> cycle for offshore gas turbine application. *Energy Convers. Manag.* **2018**, *172*, 212–227. [[CrossRef](#)]
- Moroz, L.; Burlaka, M.; Rudenko, O.; Joly, C. Evaluation of gas turbine exhaust heat recovery utilizing composite supercritical CO<sub>2</sub> cycle. In Proceedings of the International Gas Turbine Congress, Tokyo, Japan, 15–20 November 2015.
- Hou, S.; Zhou, Y.; Yu, L.; Zhang, F.; Cao, S. Optimization of the combined supercritical CO<sub>2</sub> cycle and organic Rankine cycle using zeotropic mixtures for gas turbine waste heat recovery. *Energy Convers. Manag.* **2018**, *160*, 313–325. [[CrossRef](#)]
- Cao, Y.; Ren, J.; Sang, Y.; Dai, Y. Thermodynamic analysis and optimization of a gas turbine and cascade CO<sub>2</sub> combined cycle. *Energy Convers. Manag.* **2017**, *144*, 193–204. [[CrossRef](#)]
- Kimzey, G. Development of a Brayton bottoming cycle using supercritical carbon dioxide as the working fluid. In *A Report Submitted in Partial Fulfillment of the Requirements for: Gas Turbine Industrial Fellowship*; University Turbine Systems Research Program: Palo Alto, CA, USA, 2012.

19. Held, T. *Waste Heat Recovery with Supercritical CO<sub>2</sub> Cycles—Challenges and Opportunities*; Technical presentation GT2012-70262 in the panel session “Application of Supercritical CO<sub>2</sub> Cycles to Power Production”; ASME Turbo Expo: Copenhagen, Denmark, 11–15 June 2012.
20. Walnum, H.T.; Nekså, P.; Nord, L.O.; Andresen, T. Modelling and simulation of CO<sub>2</sub> (carbon dioxide) bottoming cycles for offshore oil and gas installations at design and off-design conditions. *Energy* **2013**, *59*, 513–520. [[CrossRef](#)]
21. Held, T.J.; Vermeersch, M.L.; Xie, T.; Miller, J.D. Heat Engines With Cascade Cycles. World Patent WO/2011/119650 A2, 29 September 2011.
22. Wright, S.A.; Davidson, C.S.; Scammell, W.O. Thermo-economic analysis of four sCO<sub>2</sub> waste heat recovery power systems. In Proceedings of the 5th International Symposium on Supercritical CO<sub>2</sub> Power Cycles, San Antonio, TX, USA, 29–31 March 2016.
23. Cho, S.K.; Kim, M.; Baik, S.; Ahn, Y.; Lee, J.I. Investigation of the bottoming cycle for high efficiency combined cycle gas turbine system with supercritical carbon dioxide power cycle. In Proceedings of the ASME Turbo Expo 2015: Turbine Tech. Conf. and Exposition, Article No. 43077, Montréal, QC, Canada, 15–19 June 2015.
24. Huck, P.; Freund, S.; Lehar, M.; Peter, M. Performance comparison of supercritical CO<sub>2</sub> versus steam bottoming cycles for gas turbine combined cycle applications. In Proceedings of the 5th International Symposium on Supercritical CO<sub>2</sub> Power Cycles, San Antonio, TX, USA, 29–31 March 2016.
25. Kim, M.S.; Ahn, Y.; Kim, B.; Lee, J.I. Study on the supercritical CO<sub>2</sub> power cycles for landfill gas firing gas turbine bottoming cycle. *Energy* **2016**, *111*, 893–909. [[CrossRef](#)]
26. Kim, Y.M.; Sohn, J.L.; Yoon, E.S. Supercritical CO<sub>2</sub> Rankine cycles for waste heat recovery from gas turbine. *Energy* **2017**, *118*, 893–905. [[CrossRef](#)]
27. Marchionni, M.; Bianchi, G.; Tassou, S.A. Techno-economic assessment of Joule-Brayton cycle architectures for heat to power conversion from high-grade heat sources using CO<sub>2</sub> in the supercritical state. *Energy* **2018**, *148*, 1140–1152. [[CrossRef](#)]
28. Wu, C.; Yan, X.-J.; Wang, S.-S.; Bai, K.-L.; Di, J.; Cheng, S.-F.; Li, J. System optimisation and performance analysis of CO<sub>2</sub> transcritical power cycle for waste heat recovery. *Energy* **2016**, *100*, 391–400. [[CrossRef](#)]
29. Wang, S.-S.; Wu, C.; Li, J. Exergoeconomic analysis and optimization of single-pressure single stage and multi-stage CO<sub>2</sub> transcritical power cycles for engine waste heat recovery: A comparative study. *Energy* **2018**, *142*, 559–577. [[CrossRef](#)]
30. Astolfi, M.; Alfani, D.; Lasala, S.; Macchi, E. Comparison between ORC and CO<sub>2</sub> power systems for the exploitation of low-medium temperature heat sources. *Energy* **2018**, *161*, 1250–1261. [[CrossRef](#)]
31. Lazzaretto, A.; Toffolo, A. A method to separate the problem of heat transfer interactions in the synthesis of thermal systems. *Energy* **2008**, *33*, 163–170. [[CrossRef](#)]
32. Lazzaretto, A.; Manente, G. Analysis of superimposed elementary thermodynamic cycles: From the Brayton-Joule to advanced mixed (auto-combined) cycles. *Int. J. Thermodyn.* **2009**, *12*, 123–130.
33. Morandin, M.; Toffolo, A.; Lazzaretto, A. Superimposition of elementary thermodynamic cycles and separation of the heat transfer section in energy systems analysis. *J. Energy Resour. Technol.* **2013**, *135*, 021602. [[CrossRef](#)]
34. Lazzaretto, A.; Manente, G.; Toffolo, A. SYNTHSEP: A general methodology for the synthesis of energy system configurations beyond superstructures. *Energy* **2018**, *147*, 924–949. [[CrossRef](#)]
35. Toffolo, A. A synthesis/design optimization algorithm for Rankine cycle based energy systems. *Energy* **2014**, *66*, 115–127. [[CrossRef](#)]
36. Manente, G.; Fortuna, F.M. Supercritical CO<sub>2</sub> power cycles for waste heat recovery: A systematic comparison between traditional and novel layouts with dual expansion. *Energy Convers. Manag.* **2019**, *197*, 111777. [[CrossRef](#)]
37. Vivian, J.; Manente, G.; Lazzaretto, A. A general framework to select working fluid and configuration of ORCs for low-to-medium temperature heat sources. *Appl. Energy* **2015**, *156*, 727–746. [[CrossRef](#)]
38. Saravanamuttoo, H.I.H.; Rogers, G.F.C.; Cohen, H.; Straznicky, P.V.; Nix, A.C. *Gas Turbine Theory*, 7th ed.; Pearson Education Limited: Harlow, UK, 2017.
39. Heywood, J.B. *Internal Combustion Engine Fundamentals*, 2nd ed.; McGraw-Hill Education: New York, NY, USA, 2018.

40. Shiferaw, D.; Montero Carrero, J.; Le Pierres, R. Economic analysis of SCO<sub>2</sub> cycles with PCHE Recuperator design optimization. In Proceedings of the 5th International Symposium on Supercritical CO<sub>2</sub> Power Cycles, San Antonio, TX, USA, 28–31 March 2016.
41. Naderi, C.; Rasouli, E.; Narayanan, V. Design and Performance Characterization of a Micro-pin fin sCO<sub>2</sub> Recuperator. In Proceedings of the 6th International Symposium on Supercritical CO<sub>2</sub> Power Cycles, Pittsburgh, PA, USA, 27–29 March 2018.
42. Kemp, I.C. *Pinch Analysis and Process Integration*, 2nd ed.; Butterworth-Heinemann: London, UK, 2007.
43. Rasouli, E.; Subedi, S.; Montgomery, C.; Mande, C.W.; Stevens, M.; Narayanan, V.; Rollett, A.D. Design and Performance Characterization of an Additively Manufactured Primary Heat Exchanger for sCO<sub>2</sub> Waste Heat Recovery Cycles. In Proceedings of the 6th International Symposium on Supercritical CO<sub>2</sub> Power Cycles, Pittsburgh, PA, USA, 27–29 March 2018.
44. Cich, S.D.; Moore, J.; Mortzheim, J.P.; Hofer, D. Design of a supercritical CO<sub>2</sub> compressor for use in a 10 MWe power cycle. In Proceedings of the 6th International Symposium on Supercritical CO<sub>2</sub> Power Cycles, Pittsburgh, PA, USA, 27–29 March 2018.
45. Wright, S.A.; Radel, R.F.; Vernon, M.E.; Rochau, G.E.; Pickard, P.S. *Operation and Analysis of a Supercritical CO<sub>2</sub> Brayton Cycle*; Sandia Report, SAND2010-0171; Sandia National Laboratories: Springfield, VA, USA, 2010.
46. Noall, J.S.; Pasch, J.J. Achievable Efficiency and Stability of Supercritical CO<sub>2</sub> Compression Systems. In Proceedings of the 4th International Symposium on Supercritical CO<sub>2</sub> Power Cycles, Pittsburgh, PA, USA, 9–10 September 2014.
47. Zhou, K.; Wang, J.; Xia, J.; Guo, Y.; Zhao, P.; Dai, Y. Design and performance analysis of a supercritical CO<sub>2</sub> radial inflow turbine. *Appl. Therm. Eng.* **2020**, *167*, 114757. [[CrossRef](#)]
48. Zhou, A.; Li, X.-S.; Ren, X.-D.; Song, J.; Gu, C.-W. Thermodynamic and economic analysis of a supercritical carbon dioxide (S-CO<sub>2</sub>) recompression cycle with the radial-inflow turbine efficiency prediction. *Energy* **2019**. in Press. [[CrossRef](#)]
49. White, M.T.; Sayma, A.I. A preliminary comparison of different turbine architectures for a 100 kW supercritical CO<sub>2</sub> Rankine cycle turbine. In Proceedings of the 6th International Symposium on Supercritical CO<sub>2</sub> Power Cycles, Pittsburgh, PA, USA, 27–29 March 2018.
50. Span, R.; Wagner, W. A New Equation of State for Carbon Dioxide Covering the Fluid Region from the Triple-Point Temperature to 1100 K at Pressures up to 800 MPa. *J. Phys. Chem. Ref. Data* **1996**, *25*, 1509–1596. [[CrossRef](#)]



© 2020 by the authors. Licensee MDPI, Basel, Switzerland. This article is an open access article distributed under the terms and conditions of the Creative Commons Attribution (CC BY) license (<http://creativecommons.org/licenses/by/4.0/>).